ISSN: 2639-0108

Research Article

Advances in Theoretical & Computational Physics

# Blood Flow Dynamics through Atherosclerosis Affected and Stented Arteries

**Shafiullah Mohammad[1] and Pradip Majumdar[2]***

[1]*Department of Mechanical Engineering, Northern Illinois University, USA*

[2]*DSinnovtech Inc., USA*

***Corresponding Author**
Pradip Majumdar, DSinnovtech Inc., USA.

**Submitted:** 2024, Jan 22; **Accepted:** 2024, Feb 27; **Published:** 2024, Apr 04

**Citation:** Mohammad, S., Majumdar, P. (2024). Blood Flow Dynamics through Atherosclerosis Affected and Stented Arteries. *Adv Theo Phy, 7*(2), 01-24.

## Abstract

*Atherosclerosis is a vascular disease that reduces arterial lumen size through plaque deposition and arterial wall thickening. The pathological complications of atherosclerosis, namely heart disease and stroke, remain the leading cause of mortality in the world. The most common interventional procedure against atherosclerosis involves the placement of an intravascular stent, which is small tube-like structures placed into stenotic arteries to restore the blood flow. The flow patterns in the arteries are highly modulating along with the cardiac cycle and a strong function of the waveform created by the heartbeat. In this study Computational Fluid Dynamics (DFD) Analysis is performed on the femoral artery with an objective to evaluate the design of stents and its impact on blood flow dynamics. Simulations are performed on healthy, atherosclerosis affected and stented femoral arteries. Velocity and wall shear stress fields over the cardiac cycle are analyzed to predict the outcome of the interventions in terms of recirculation and stagnation regions and identify improved stent designs. The complex blood flow pattern with slow moving regions, flow separation and recirculatory form near the wall during cardiac cycle is the major contributing factor to the formation of the atherosclerotic plaque at that location. It was demonstrated that adverse flow field created upstream and downstream of the blockage may cause enhanced growth in size of the blockage. The stent design also plays a significant role in the possibility of restenosis.*

**Nomenclature**

| | |
|---|---|
| BPM | Beats per minute |
| CFD | Computational Fluid Dynamics |
| CT | Computed tomography |
| D | Diameter of the tube |
| DES | Drug Eluting Stents |
| F | Frequency |
| FSI | Fluid structural interaction |
| P | Pressure |
| $\frac{dp}{dz}$ | Pressure Drop |
| Q | Volumetric Flow |
| T | Time in sec |
| $U_{cl}$ | Centerline velocity |
| U | Velocity |
| $V_F$ | Systolic forward peak velocity |
| $V_R$ | Diastolic reverse peak velocity |
| $V_D$ | End of diastolic velocity |
| $V_M$ | Time – average mean velocity. |
| WSS | Wall Shear Stress |

**Greek Symbols:**

| | |
|---|---|
| τ | Shear stress |
| α | Womersley Parameter |
| υ | Kinematic Viscosity |
| μ | Dynamic viscosity |
| ρ | Density of liquid |

## 1. Introduction

Atherosclerosis is a vascular disease that reduces the arterial lumen size through plaque deposition and arterial wall thickening. The pathological complications of atherosclerosis, namely heart disease and stroke, remain the leading cause of mortality in the world. The most important reason for stroke is Stenosis in the coronary artery, it blocks the oxygen supply to organs, and it can cause paralysis of organs. Atherosclerosis can affect all large and medium sized arteries of the body, coronary, carotid, cerebral and femoral arteries. There are more chances of forming at branches and bends within the cardiovascular system. The atherosclerotic plaques contain lipids, inflammatory cells, smooth muscle cells and connective tissue. Risk factors for this disease are diabetes, cigarette smoking, family history, sedentary lifestyle, obesity, and hypertension. Other than these factors, the presence of local hemodynamic factors such as wall shear stress plays a major role in the generation of atherosclerotic plaques. The common interventional procedure against atherosclerosis involves the placement of an intravascular stent. A stent is a small metal medical device that restores the blood flow perfusion to the downstream arteries. Stents are tubular mesh structures which are inserted in a stenotic artery using a medical procedure that carries it on a balloon and expanded until they deform plastically to provide stiffness to hold the arteries from collapsing. Atherosclerosis is developed at the bifurcation of the artery which leads to stroke for the patients. Computational fluid dynamics can be used to find the local velocity distribution and wall shear stresses to predict the atherosclerotic plaque formation areas.

The transient phenomenon of blood flow is a result of the cyclic nature of the heart. That is at a given point the velocity and pressure conditions change with time. In the circulatory system the blood velocity is pulsating in nature; it varies in between zero during diastole and high velocities during systole. Blood flow is laminar flow, but because of its pulsating nature of the flow makes it turbulent when the artery diameter and velocities are large for the arteries like aorta. These complex hemodynamic characteristics of blood flow play an important role in forming the atherosclerotic plaques. Blood flow in human arteries is also well known for its unsteadiness, and hence the Computational Fluid Dynamics (CFD) model is well suited for the computation of the complex unsteady nature of the hydrodynamic flows that vary extremely along the cardiac cycle. Blood is also a complex mixture of red blood cells and white blood cells; it is non-Newtonian fluid involving non-liner stress-strain relations. Another important fact is the flexibility and deforming nature of the arterial walls. Collecting all these complex characters and implementing them in one CFD model is a difficult task.

One of the significant attempts to model the blood flow in vessels was performed by Womersley [1]. He analyzed the equations of viscous motion for laminar flow by considering blood as a Newtonian, incompressible fluid, and artery as an infinitely long and straight circular tube. The main purpose of his study was to calculate the velocity and flow rates in arteries with a given pressured pressure gradients as given by McDonald [2,3]. The pressure gradient obtained by McDonald was represented as a Fourier series to compute the velocity profiles.

Ku [4] has given a brief introduction of cardiovascular system, blood properties, heart functionality, arterial tree, velocity profiles, flow in specific arteries, initiation of atherosclerosis and biological responses to hemodynamic.

Silva [5], has simulated abdominal aorta and renal branches for both idealized and realistic geometry obtained from CT images of a normal adult subject and using the waveform calculated by Taylor and Droney [6]. They performed operations on two different configurations of inlet velocity boundary conditions, uniform velocity, or a fully developed velocity profile. Results demonstrated similar velocity distributions for both uniform and fully developed boundary conditions. They found the recirculation zone at the proximal wall of renal branches and along the posterior wall of the abdominal aorta.

Pant [7] did experiments on five different coronary stent designs used in clinical practice. Results show that the cardiac pulse at different points on pulsating pressure wave produce different responses to the stent when measured by artery wall areas exposed to low Wall Shear Stress (WSS) and reverse flow. The flow differences exist when both these factors are considered simultaneously. The areas with local wall shear stress (WSS) magnitude of less than 5 dynes/cm2 show most initial thickening of deposit. The hemodynamic alteration, measured by percentages of areas exposed to low and reverse WSS, is proportional to the length of the stent connector in the cross-flow direction.

Jin [8] has performed CFD analysis by combining the Computed Tomography (CT) slices in a human left coronary artery. They performed X-ray CT scanning of the left coronary artery and aortic root of a healthy volunteer. The velocity waveform used in this study was calculated by using MRI scanning of a coronary artery of a healthy male volunteer. They observed that the middle section of the left main coronary artery experiences high WSS during the peak time of the cardiac cycle. They also observed that the myocardial side of the separation region exhibits low WSS because of the inner curvature of the coronary artery, this region implies the higher probability of plaque formation.

Dehlaghi [9], computed the blood pressure waveforms in three different sites: pre-stent, middle of stented arterial segment and post-stent regions using CFD. They worked on the effect of stent geometry on blood flow patterns, and they concluded that the blood flow patterns are strongly affected by the stent design. The phase shift between pressure and flow waveform were studied on different stents designs and concluded that the phase lag is a function of Womersley parameter α and stent geometry. The stent strut with elliptical geometry is more effective than those with hexagonal and rectangular geometries.

Xiaoyi [10] developed a computer code using Mathematica software to perform a series of computer simulation experiments and to compare the effects of different waveform shapes on the velocity profiles for unsteady flow. The input to this code could be any of the flow properties such as pressure gradient, flow rate, centerline velocity or the shear stress.

Hashimoto [11] performed the flow pulse wave analysis on 138 patients of ages 56±13 by recording 16-sec data of the femoral flow velocity. They interpolated the velocity data for every 10ms and plotted against time using a code written in Mathematica Software. The beat-to-beat pulse waveforms were put together and averaged for ten consecutive pulses i.e., over ten cardiac cycles and generated an averaged femoral velocity waveform.

Wong [12] have performed CFD simulation using a bend section of a stented atherosclerotic artery with two 6mm stent segments and one *48mm* stent and concluded that the full-length stent experienced significantly higher stresses than the two 6-mm segments in a bend section of an atherosclerotic artery.

Shaik [13] has investigated the difference in results based on Newtonian and non-Newtonian fluid flow using CFD for two different three-dimensional models of an artery. The effect of arterial geometry on the flow field is analyzed in terms of the development of atherosclerosis in arteries. Their results show small effect of non-Newtonian cous property relation on velocity profiles but show significant difference in the in the wall shear stress. The geometry of the artery plays a significant role in locating the atherosclerosis in the arteries.

Dehlaghi [14], performed simulations on stented coronary artery with a flow divider in three different sites including stented, pre-stented and post stented, and concluded that the wall shear stress between stent struts was sensitive to strut spacing, profile of the strut, number of struts and curvature. They suggested that the stent strut with elliptical geometry is more appropriate. Wall shear stress depends strongly on the presence and diameter of the flow divider in stented segment.

Yang [15] has investigated the effects of stent in different types of stented cerebral artery model. They modeled the blood vessels as straight, curve and y-branch shape. They limited their study to steady flow with velocity of 0.43m/sec. They observed the stress on the blood vessel wall by stenosis can be reduced by implementing a stent.

Valencia [16] has performed numerical simulation on the unsteady non-Newtonian blood flow and mass transfer in symmetric and non-symmetric stenotic arteries, considering the Fluid structure interaction (FSI) using the code ADINA. They performed numerical investigation on FSI of eight stenotic artery models with symmetric and non-symmetric arteries by varying the percentage of restriction and the respective eight stenotic artery models with rigid walls. Their results concluded that the artery with rigid walls is not realistic, as the artery is dilated and compressed in cardiac cycle.

Cole [17] has performed CFD simulations of blood flow through a typical three-dimensional human femoral artery bypass graft models by considering blood as non-Newtonian fluid. They performed simulations on both steady and unsteady inlet conditions. Their steady flow simulations have demonstrated that the flow patterns at the anastomoses are very strongly influenced by the configuration geometry. At larger anastomotic angles, flow disturbances are augmented. They presented the importance of modeling the complete bypass configuration, rather than simply the proximal or distal anastomosis in isolation by observing the flow within the graft does not attain fully developed nature.

In this study, Computational Fluid Dynamics (DFD) Analysis is performed on the stented femoral artery femoral artery with an objective to evaluate the design of stents and its impact on blood flow dynamics. Objective is to analyze and characterize pulsating blood flow conditions within the artery with and without plaque formation, and with the inclusion of a stent by considering blood flow as a pulsating, incompressible and Newtonian fluid. The arterial wall is limited to rigid and straight tube with a branch. The governing transient Navier-Stokes equations are solved by using a commercial simulation software code Star-CCM+. Unsteady simulations are run for a pulsating velocities range consisting of both diastole and systole phases according to the pulsating waveform for the femoral artery. The computational simulation model is validated by comparing results with the limiting case fully developed analytical series solution for pulsating blood flow in a straight section as presented by Womersley [1]. The velocity waveform generated by Hashimoto [11] is used as an inlet boundary condition for the rest of the current computational study. The velocity, pressure and stress fields over the artery are analyzed to predict the outcome of the interventions in terms of recirculation, stagnation regions, and identify the possibilities of plaque formation and failure of the artery. A number of stent designs are evaluated in terms of flow conditions and to identify improved stent designs and treatment techniques.

## 2. Blood Circulatory System and Physical Problem

In this section, a brief description of the cardiovascular system and characteristics of the blood flow dynamics is given. Causes of atherosclerosis, treatment techniques and design of stents that are used in the treatment of this disease are discussed. Further, the physical model of the blood artery system that is considered for flow analysis is presented. All input cardiac cyclic velocity and pressure conditions and relevant parameters are also described.

### 2.1. Cardiovascular System and Cardiac Cycle

The cardiovascular system is a complex structure that prominently supplies oxygen and nutrients to the body organs and aids in the removal of waste products that are generated during the process of metabolism from tissue cells. A cardiovascular system significantly comprises of a heart and a circulatory system made up of large and small elastic vessels that transport the blood throughout the body. The heart is the main organ of the cardiovascular system. As the muscular walls of the heart beats or contract continuously, blood gets pumped to all parts of the body. Figure 1 shows the interior cut-out view of a human heart [18]

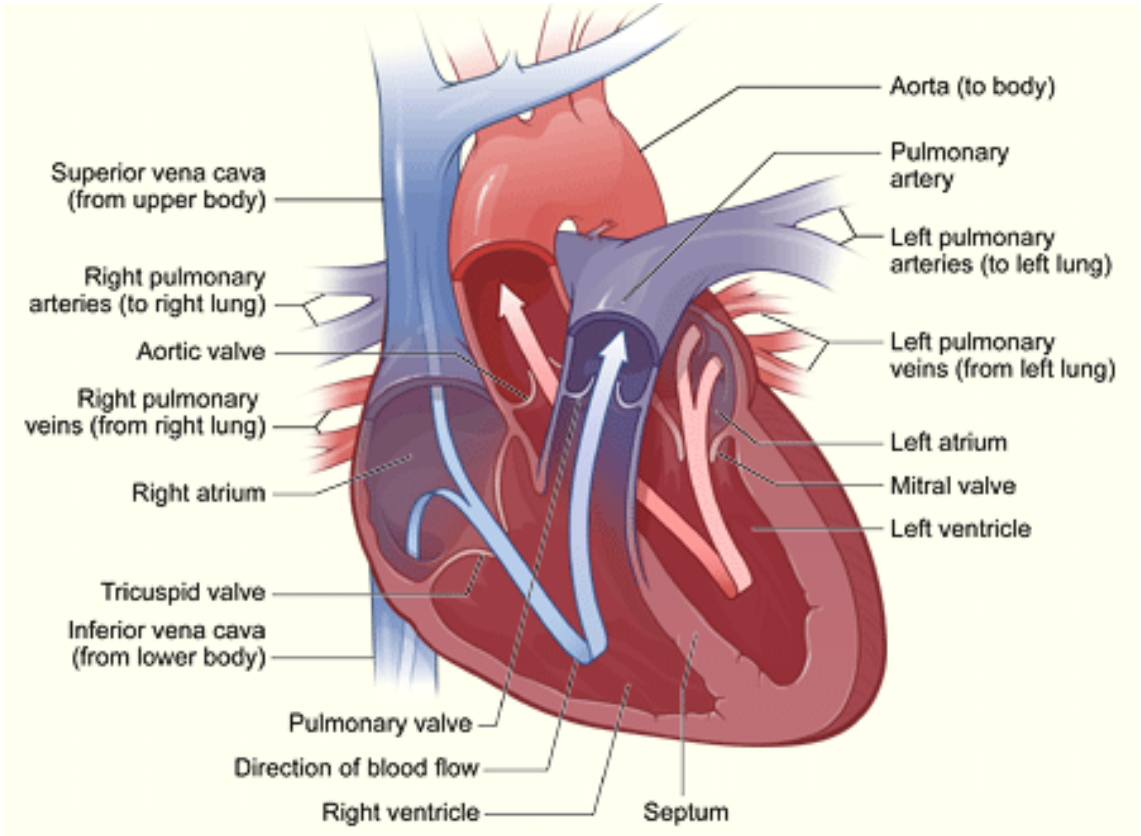


**Figure1:** Interior cut-out view of a human heart [18]

The heart has four chambers: the right and left atria are in the upper part of the heart, and these receive and collect blood The right and left ventricles located in lower part of the heart, and these pump blood out of your heart into the circulatory system to other parts of your body. As depicted in the Figure, heart has four valves: the aortic valve, the tricuspid valve, the pulmonary valve, and the mitral valve. These valves allow pumped blood to pass through the chambers and into the arteries without backing up or flowing backward, acting like a check valve. The ventricle on the right side of the heart pumps blood from the heart to the lungs. When a person breathes in air, oxygen passes from the lungs through the blood vessels and into the blood. Carbon dioxide, a waste product, is passed from the blood through blood vessels to the lungs and is removed from the body when breathed out. The left atrium receives oxygenated blood from the lungs. Blood from the left atrium is pumped to left ventricle from where the blood is pumped to the rest of the body through the aorta.

Electrical activity causes the rhythmic contraction and relaxation of the hearts chambers and produces the so-called cardiac cycle, which consists of two phases: Diastole phase and Systole phase. During the diastole phase, the heart relaxes allowing blood to enter the heart, and blood is ejected during systole phase. The heart beats correspond to the closure of the valves and depends on heat conditions and blood flow dynamics. While a normal heart beats at a rate between 60-100 beats per min, the heart rate varies depending upon various factors like age, gender, and health. The pulse rates increase with the breathing rate, physical exercises (aerobic), digestion, excitement, and any kind of physical exertion, affecting the heartbeat count.

### 2.2. Circulatory System

The circulatory system is an intricate network of vessels that supplies blood to all body organs and tissues. Blood flows into the organs and tissues of the body through arteries and collected back from them through veins. Oxygenated blood from the heart is pumped into the aorta, blood from the aorta is pumped into the blood vessels called arteries which are further branched into smaller tubes called arterioles and these arterioles divide into capillaries. The capillaries carrying deoxygenated blood are merged into venules which carry impure blood and venules further form veins. Walls of larger and medium sized arteries are lined by connective tissue, muscle, and endothelium while capillaries are lined by endothelium alone. The exchange of oxygen, metabolic wastes and carbon dioxide occurs in the capillaries. A large part of waste is extracted from the blood as it flows through the kidneys. Arteries adapt to varying flow and pressure conditions by enlarging or shrinking to meet the changing hemodynamic demands. Some of the important arteries vary in size from 3-mm to 16-mm. Some of the important arteries including femoral artery and veins in the human body are shown in figure 2. The figure also illustrates the detail network of the arteries and veins in a human circulatory system including the section on femoral artery considered in this study.

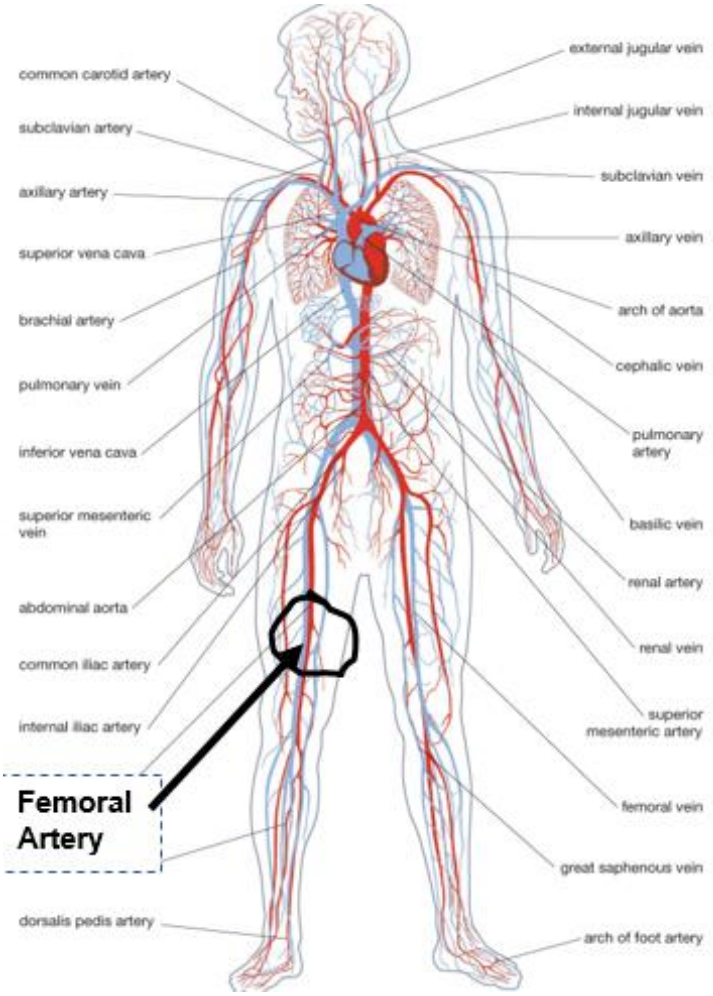


**Figure 2:** A detail network of arteries and vein a human blood circulatory system [encyclopedia: https://cdn.britannica.com/49/115249-050-0DFBBCD3/Human-circulatory-system.jpg [19]

### 2.3. Flow Parameters:

Some of the most important flow parameters that strongly impact blood flow dynamic are Womersley number and the Reynolds numbers, which are briefly discussed here. The unsteady flow through the entrance region depends on the Womersley parameter and the Reynolds number.

### 2.4. Womersley Number

The dimensional analysis of unsteady Navier-Stokes equation leads to a non-dimensional number known as Womersley parameter. Womersley parameter is defined as the ratio of unsteady inertia forces to the viscous forces as defined by the following equation:

$$\alpha = \frac{D}{2}\sqrt{\frac{2\pi\rho f}{\mu}} \qquad (1)$$

Where D is the tube diameter,  is the density of the fluid and μ is the dynamic viscosity and f is the frequency of the wave form.

For low Womersley numbers the viscous forces are high, and the velocity profiles are expected to be more parabolic, and the centerline velocity oscillates in phase with the driving pressure gradient. For high Womersley numbers (>10), the unsteady inertial forces are high compared to viscous force and this results in considerably flatter velocity profile and a phase difference between with the pressure gradient.

### 2.5. Reynolds Number

The typical Reynolds number of blood flow in arteries varies from 1 to 1000 in small arterioles and approximately 4000 in big arteries like aorta.

### 2.6. Blood Flow Types

Blood is a complex fluid characterized by the suspension of cellular elements, namely, red blood cells (erythrocytes), white blood cells (leukocytes) and platelets in the plasma circulating in a cardiovascular system. Red blood cells typically comprise approximately 40% of the blood by volume. Because red blood cells are small semisolid particles, they increase the viscosity of blood and affect the behavior of the fluid. Moreover, blood does not exhibit a constant viscosity at all flow rates and is especially non-Newtonian in micro circulatory system. The non-Newtonian behavior is most evident at exceptionally low shear rates when the red blood cells clump together into larger particles. Blood also exhibits non-Newtonian behavior in small branches and capillaries. However, in most arteries, blood behaves in a Newtonian fashion, and the viscosity is assumed as a constant. Blood flow and pressure are unsteady due to the cyclic nature of the heart operation that creates pulsating conditions in all

arteries and have characteristic of pulsatile shapes that vary in different parts of the arterial system.

### 2.7. Femoral Artery Waveform

The waveform used in the analytical and CFD solution is based on a femoral artery wave form. This waveform is generated by the 16 sec data of the femoral flow velocity interpolated offline for every 10ms and plotted against time using Mathematica Software. The beat-to-beat pulse waveform was ensemble-averaged for ten cardiac cycles (i.e., ten pulses) and an averaged waveform for the flow velocity is generated. Figure 3 shows a typical velocity waveform in a femoral artery.

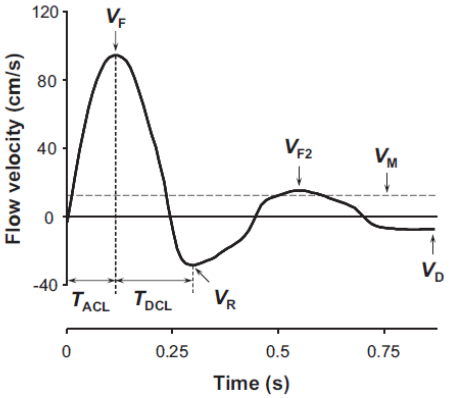


**Figure 3:** A typical femoral artery wave form.

The waveform for flow velocity is described in terms of the following parameters: Systolic forward peak velocity ($V_F$), Diastolic reverse peak velocity ($V_R$), End diastolic velocity ($V_D$) and Time-averaged mean velocity ($V_M$). The femoral flow velocity increased rapidly in early systole and reached peak velocity ($V_{F2}$) and it reduces gradually to the minimum reverse velocity ($V_R$). The deceleration time is comparatively shorter than the acceleration time. The amplitude of the reverse flow velocity is smaller than the forward flow velocity and greater than the diastolic flow velocity.

### 2.8. Temporal variation of Velocity profile in arteries

Blood flow and pressure are unsteady and pulsating. The cyclic nature of the heart pump creates pulsating le condition in all arteries. The heart ejects and fills blood in alternating cycles called systole and diastole. Pressure and flow have characteristic pulsatile shapes that vary in different parts of the arterial system. A physiologic flow waveform can be expanded as a Fourier series, and the harmonic components of velocity can be summed to unsteady velocity profiles. Fully developed pulsating flow in a straight tube is explained by Womersley [2].

The flow is not fully developed near some of the regions of arteries. The flow in these regions is like entrance flow and a developing layer at the wall. The velocity profiles are blunt at the center. Unsteady flow through the entrance region depends on the Womersley parameter and the Reynolds number. For a medium-sized artery the Reynolds number is around 10-1000 and the Womersley number is 1-10. Solving Navier-stokes equations for these types of arteries is simple when compared to the other arteries. In these types of cases the effect of elasticity is small, so the artery can be assumed as the rigid tube.

### 2.9. Atherosclerosis and Use of Stent

Atherosclerosis is a vascular disease that reduces arterial lumen size through plaque formation and arterial wall thickening. The complications of atherosclerosis are namely heart disease and stroke. Figure 4 shows the difference between the healthy artery and atherosclerosis affected artery.

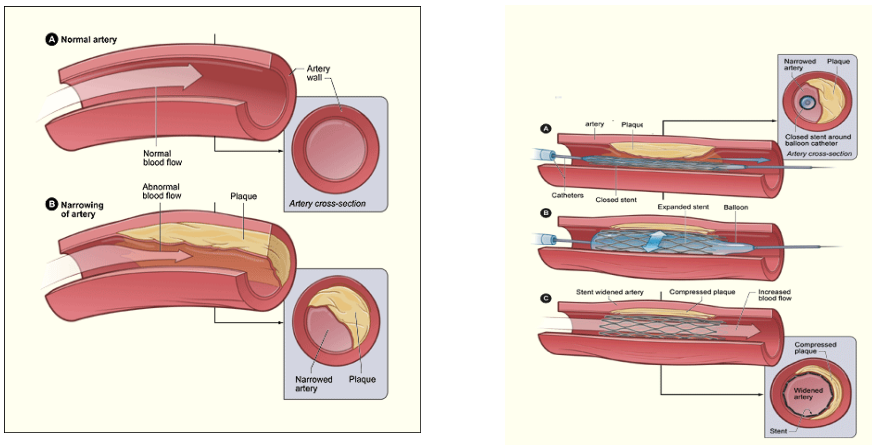


(a) (b)

**Figure 4:** (a) shows a normal artery with normal blood flow and (b) shows an artery with plaque buildup.

A common percutaneous coronary procedure such as balloon angioplasty and balloon expandable stents involves the placement of an intravascular stent and are used against advanced atherosclerosis. An intravascular stent is a small tube-like structure that can be placed into stenotic artery to restore blood flow. A stent is a small tube-like structure that can be placed into the stenotic artery to restore blood flow and perfusion.

There are different types of stent designs, made of different materials using different fabrication methods, and manufactured by number of different companies [Watson et. al (20); Schmitz et. al (21); Warzyrfska et. al (22); Stoeckel et. al ( 23)]. Most recent designs include coatings and drug-eluting stents (DES) that prevent restenosis [Noad et. al (24), Schmidt and Abbott (25)].

Stoeckel et. al [23 ], in their survey study of stents designs, differentiated various aspects of stent design such as raw material forms, geometrical features, fabrication methods and additive stent surface coatings and layers. Noad et. al [24] discussed the clinical impact of the stent design considering implication of the demands for thinner stents while sustaining the mechanical properties like radial strength of the stent. Schmidt and Abbott [25] presented a review study of the technological progress in the design and construction of stents and on deployment of balloon expandible stents. This discussion covers the stent properties and use of metal alloys, polymers, bioresorbable vascular scaffolds and drug elution.

Major characteristics of stents are the size representing the wall coverage, material of construction, strut thickness and spacing, struct mesh pattern and type of connectors. Over the years stainless steel was the most common stent material due to its higher structural strength. However, in recent times, other alloys like cobalt, chrome, chromium and platinum alloys, and polymer are used for making stents with reduced thicknesses and spacing to reduce disturbance to blood low. Stents are available with strut thickness in the range of 60-140 microns. Stent mesh patterns are of the form of sinusoidal hoops fabricated using laser cuts or connected wire coils using connectors or welding.

## 3. Limiting Case Analytical solution

The solution for homogeneous, incompressible, Newtonian fluid flow in a rigid, cylindrical tube with cardiac cyclic inlet flow conditions is given by McDonald et. al [2,3). This solution is summarized here.

The flow property based on the cardiac cycle is a periodic phenomenon and it can be expressed as the sum of a Fourier series of form.

$$\frac{dP}{dZ} = \dot{A}(\omega)e^{i\omega t} \qquad (1)$$

This is periodic in time with frequency ω. Based on this periodic pressured gradient, the axial component velocity in the straight tube is given as

$$u(r,t) = \frac{\dot{A}}{i\rho\omega}\left\{1 - \frac{j_o\left(i^{3/2}\alpha\frac{r}{R}\right)}{j_o\left(i^{3/2}\alpha\right)}\right\}e^{i\omega t} \qquad (2)$$

Where $\alpha$ is the Womersley parameter, R is the radius of the tube, $\rho$ is the density of the fluid. Based on the velocity distribution given in Eq. (), , the flow rate flow rate Q, the center line velocity $u_c$ l and the wall shear stress $\tau_w$ can be expressed as follows

$$Q = 2\pi\int_0^R ur\,dr \qquad (4)$$

$$Q = \frac{\pi R^2 \hat{A}\,\hat{A}}{i\rho\omega}\left\{1 - \frac{2}{i^{\frac{3}{2}}\alpha} * \frac{J_1 i^{\frac{3}{2}}\alpha}{J_o i^{\frac{3}{2}}\alpha}\right\}e^{i\omega t} \qquad (5)$$

$$u_{CI} = u(0,t) \qquad (6)$$

$$u_{CI} = \frac{\hat{A}}{i\rho\omega}\{1 - \frac{1}{Jo\left(i^{\frac{3}{2}}\alpha\right)}\}e^{i\omega t} \qquad (7)$$

$$\tau_\omega = -\mu\frac{\partial u}{\partial r} \quad at \quad r = R \qquad (8)$$

$$\tau_\omega = \frac{\mu\hat{A}\,\hat{A}\,i^{3/2}\alpha}{i\rho\omega R} * \frac{J_1(i^{\frac{3}{2}}\alpha)}{J_0(i^{\frac{3}{2}}\alpha)}e^{i\omega t} \qquad (9)$$

The following relationship exists between the harmonic magnitude of pressure gradient, flow rate, centerline velocity and the wall shear stress.

$$\frac{\hat{K}(\varpi)\mathrm{Re}}{i\alpha^2 J_0(i^{3/2}\alpha)} = \frac{\hat{Q}(\varpi)}{J_0(i^{3/2}\alpha) - \frac{2}{i^{3/2}\alpha}J_1(i^{3/2}\alpha)} :$$

$$= \frac{\hat{u}_{cl}(\varpi)}{J_0(i^{3/2}\alpha) - 1} = -\frac{\hat{C}_f(\varpi)\mathrm{Re}}{i^{3/2}\alpha J_1(i^{3/2}\alpha)} \qquad (10)$$

Thus, if one of the flow properties from pressure gradient flow rate centerline velocity or shear stress is known, then it is possible to obtain the other flow properties from the above equation.

### 3.1. Computational Model

A detailed description of the computational model in terms of assumptions, geometry, computational mesh, and computational parameters are given in this section. The computational model for pulsating blood flow in the artery subject to a cardiac cycle is developed based on the following assumptions: i. Ideally blood flow should be modeled as a two-phase flow with suspension of blood cells in plasma. However, such a complex model requires additional models relating the interactions of blood cells and base fluids, and computationally very time consuming. Initial development of the simulation model is primarily restricted here to single-phase blood model for first-order close realistic analysis of pulsating blood flow; iii. Blood is assumed as a Newtonian and incompressible fluid and assuming constant viscosity and density.; iii. An artery is flexible with motion and deformation of the arterial wall according to the cardiac cycle. The artery is

assumed to be a rigid tube assuming a small effect of elasticity; iv. Governing equations for the CFD model are based on Navier-Stokes equations for laminar, incompressible fluid flow and no-slip wall velocity conditions; and v. Inlet velocity is assumed to be pulsating following the velocity wave form shown in Figure 1.

Simulations were carried over a period of pulse cycle ranging from velocities below zero during diastole to a maximum of 0.95 during systole. The inlet boundary condition is given as velocity profile based on the waveform generated as shown in Figure 1.

### 3.2. Unsteady Computational Parameters

Simulation is conducted as an implicit unsteady condition with inlet velocity is given as the table of velocity and times generated by digitizing the velocity waveform as explained above. The segregated flow solver is used to solve the flow equations. Temporal discretization of first order is used to solve the problem. The maximum physical time is taken as 0.8sec and the time step of 0.01sec and 50 inner iterations were allowed for each time step. Under relaxation factor for velocity is taken as 0.7 and 0.3 for pressure.

A 3-dimensional computational model of femoral artery with the presence of branch is developed using commercial CFD software called STAR CCM+, which uses control volume-based discretization method for solving for Navier-Stokes equations to predict the unsteady flow patterns throughout the cardiac cycle. A femoral artery section was selected in this study as it is one of the regions where atherosclerotic disease is likely to occur.

### 3.3. Artery Geometry

In this study the geometry of the femoral artery was constructed based on the averaged sizes of the arteries given by Hashimoto. et.al [11]. The artery is assumed as rigid and straight by neglecting the wall motion and curvature. Three geometric models of healthy artery, stenosis affected and stented arteries are developed for analysis.

The geometry of the femoral artery tree with branch was constructed in Pro-E Creo based on the dimensions given by Hashimoto et. al [11]. In this study a part of the femoral artery tree, highlighted in Figure 5, is considered to study the flow patterns in three different modes: a healthy artery, a stenotic artery, and a stented artery.

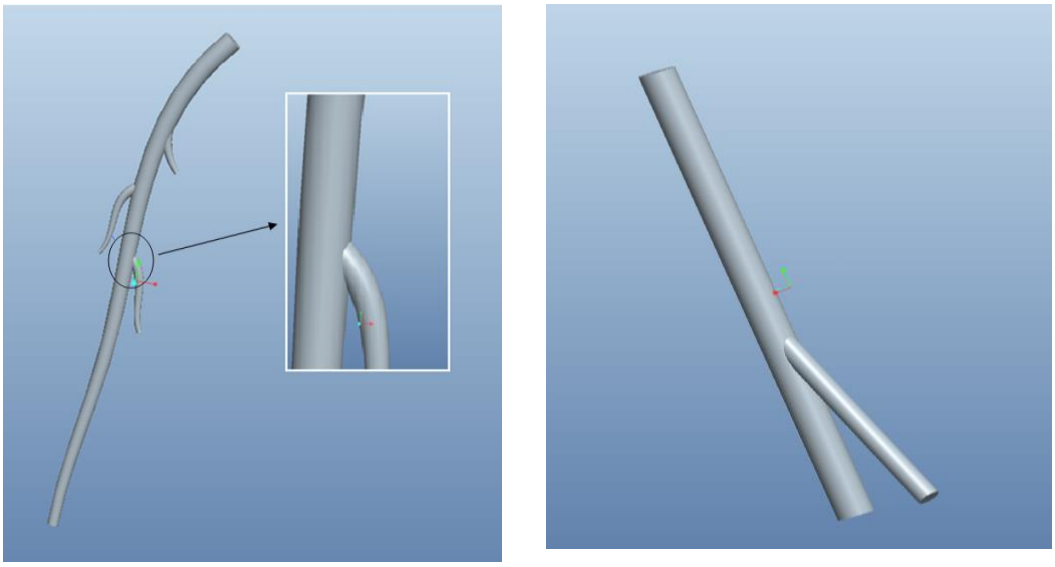

**Figure 5:** (a) Femoral artery tree with the insight view of the area under consideration
(b) Geometry of the healthy femoral artery.

The healthy femoral artery was designed by taking 120mm of length and 8mm diameter with a branch of diameter 5mm with a 25o angle to the main artery. The Stenotic region has been designed on the same artery by creating a narrow region of inner diameter of 4mm i.e., half to the diameter of the artery so that it blocks 50% of the pathway, and the stenosis region is 30mm in length. Stent is designed by crossing four spiral lines with circular cross section with radius 0.5mm, with the length of 30mm (same as the stenosis region) the stent is transferred to the healthy artery, the combination of this artery and stent is like a stent implanted on the artery. The geometric model of the idealized healthy femoral artery is as shown in Figure 5b. The length of the artery is considered 120mm with a fixed diameter of 8mm and a branch of diameter 5mm is added to it at 70mm from the base at an angle of 25o.

### 3.4. Stenosis Affected Artery

The stenosis region is created by narrowing the middle section of the artery. The stenosis of length 30mm is placed at 40mm from the inlet and the radius of the narrow section is given as 2mm. The geometric model of the stenosis affected artery is as shown in Figure 6.

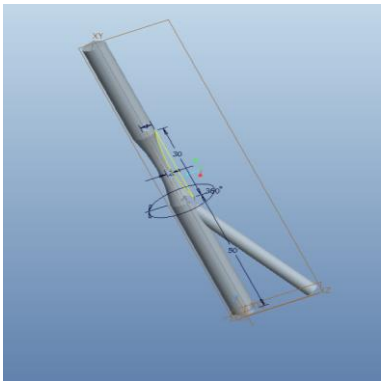

**Figure 6:** Geometry of the Stenosis effected artery.

### 3.5. Stented Artery

This stent model is designed by using the helical sweep protrusion feature in Pro-E. in this stent model, 4 spiral lines are crossed and the length of the stent is taken same as the length of the stenosis created i.e. 30mm, with the outer diameter of 8mm and the strut cross-section is taken as circular with diameter 0.5mm and two stents with 1.5mm and 3mm strut spaced stents are designed to compare the results. Figure 7 shows the stent design with 3-mm and 1.5-mm struts.

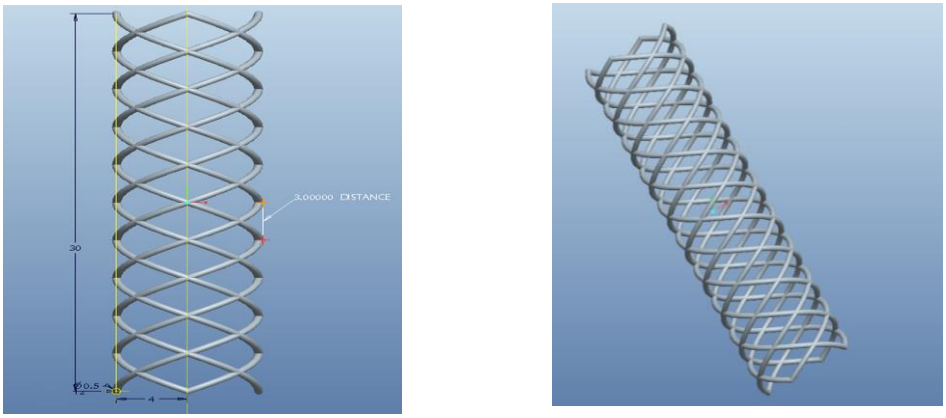


(a) Stent design with 3mm strut spacing.

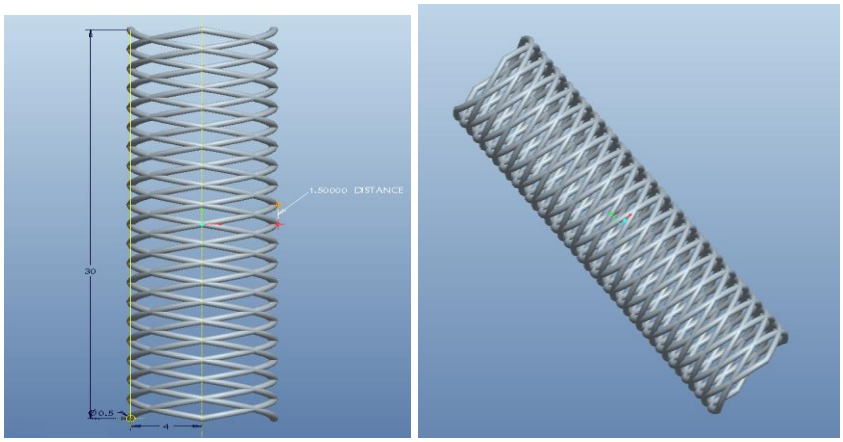


(b) Stent with 1.5mm strut spacing.

**Figure 7:** Stent design: with 1.5mm strut spacing.

This stent design is transferred to a healthy artery wall at the specified location and the combination of the artery wall, and the stent is considered as the stent implanted artery. Figure 8 shows the stent implanted on the arterial wall.

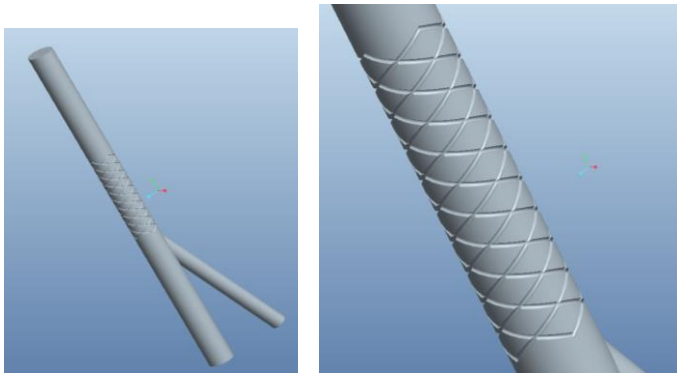

(a) 3mm strut spacing.

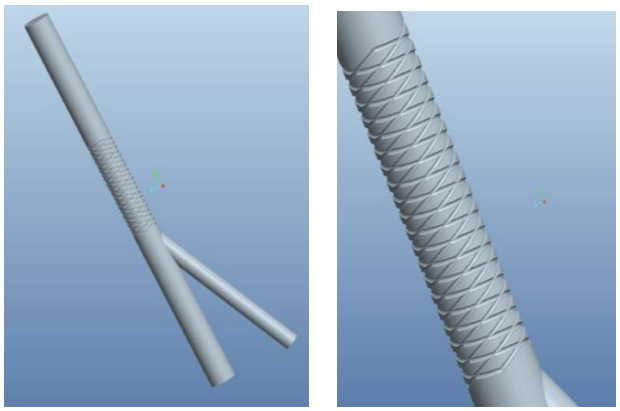

(b) 1.5mm strut spacing

**Figure 8:** Stent implanted arterial wall.

### 3.6. Mesh Generation

To resolve the complex changes in the flow field variables such as velocity, shear stresses and pressure induced by the pulsating cardiac waveform, the grid needs to be sufficiently dense.

### 3.7. Mesh for Healthy Artery

The generated mesh for the artery is as shown in Figure 9. The mesh is generated using trimmed- trimmed hexahedral cell shape-based core mesh and thin mesh- tetrahedral or polyhedral based prismatic thin mesh The base size of 0.3mm with three prism layers, and with a prism layer thickness of 25% of the core and medium temporal growth is selected.

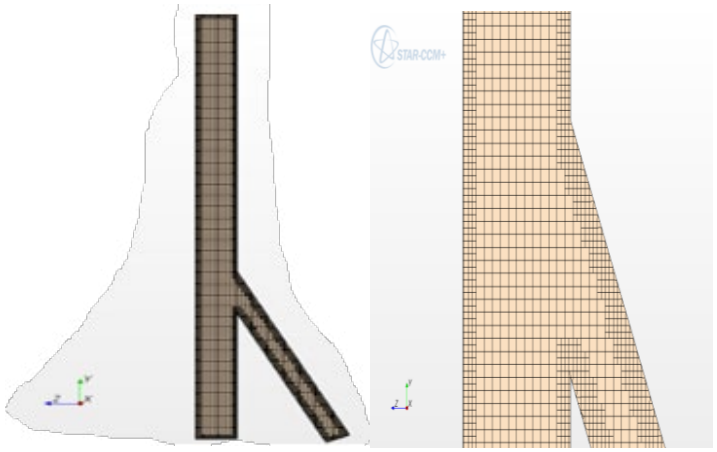

(a) Mesh for healthy artery.

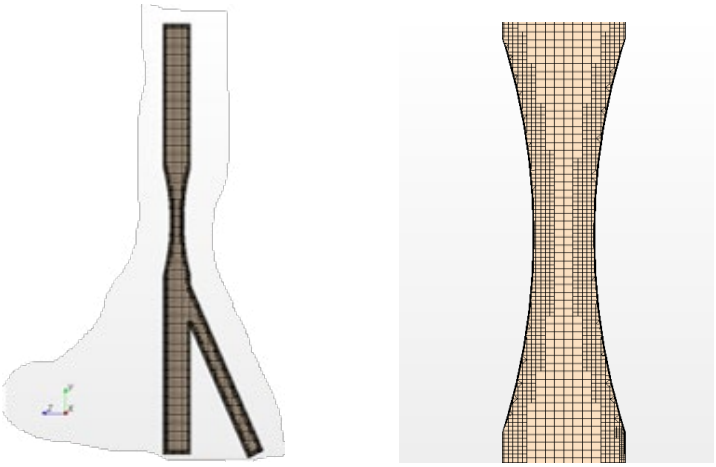

(b) Mesh for restricted artery

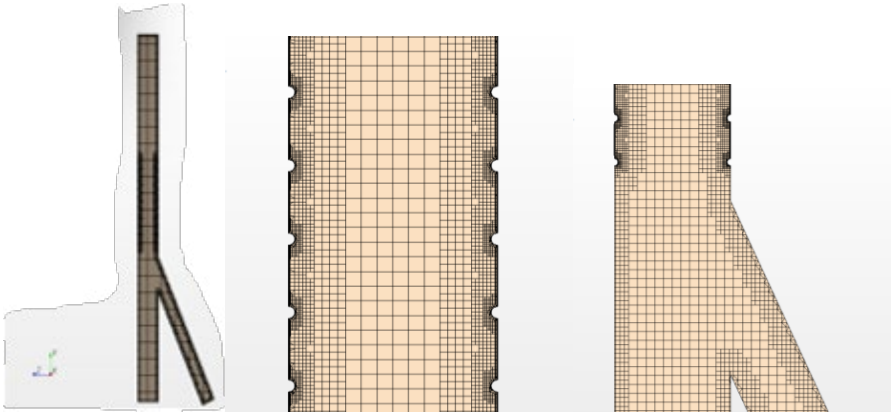

(c) Mesh for stented artery with 3mm strut space.

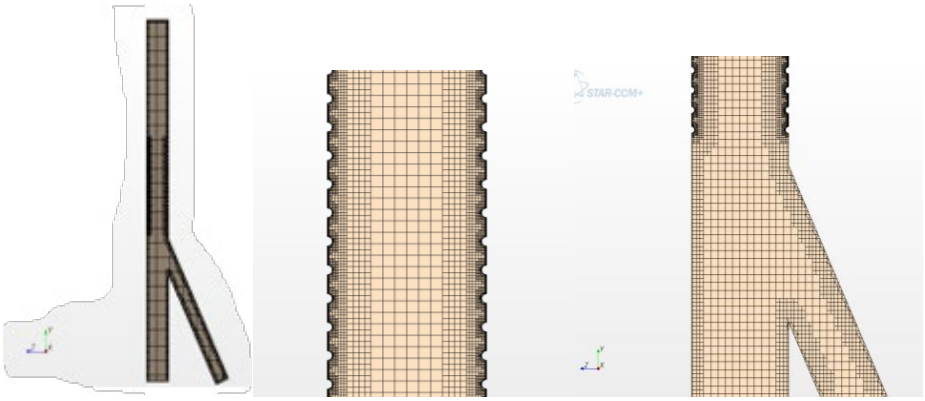

(d) Mesh for stented artery with 1.5mm strut space.

**Figure 9:** Computational mesh

### 3.8. Grid Refinement Study

A series of computational experiments have been performed by changing the base size to adopt an optimized grid. Three different base sizes are evaluated by simulating the healthy artery in the steady case, and convergence of wall shear stress (WSS) distribution at the branch wall was observed to assess the mesh quality.

## 4. Results and Discussions

### 4.1. Validation of computational solution

For validation purposes, the CFD results are compared with the limiting case analytical solution obtained for the unsteady flow through rigid pipe as presented by equations (2-10) in section -2. To perform this task, steady state entrance region simulation is performed on a straight artery to establish the fully developed flow conditions in terms of entrance length requirement. The inlet

velocity is given as 0.96m/s, which is the maximum velocity in the pulsating unsteady flow waveform. As expected, the center region of the blood flow gets accelerated while it is slowed down near the rigid wall due to no slip condition. Figure 10 shows the progressive increase in center line velocity with increase with the length of the pipe and approaches a constant centerline velocity, representing a fully developed flow condition.

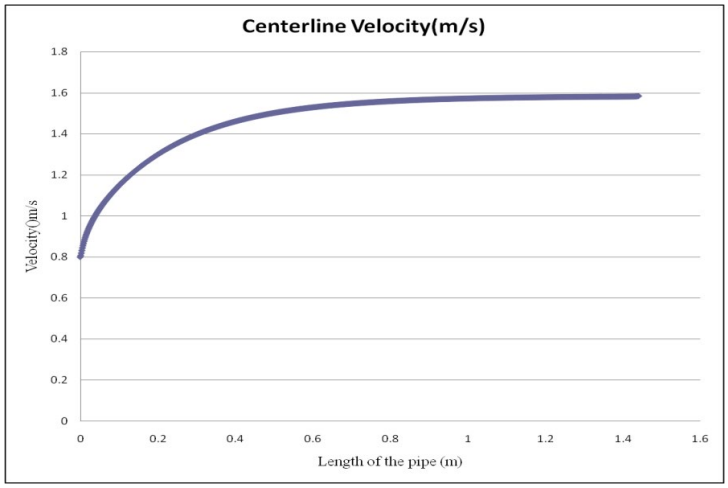


**Figure 10:** Variation of centerline velocity in the entrance region of a straight artery.

Results show a fully developed velocity condition at around 1-m distance from the entrance for the given inlet velocity. The axial velocity profiles are plotted for different locations along the length of the tube as shown in Figure 11.

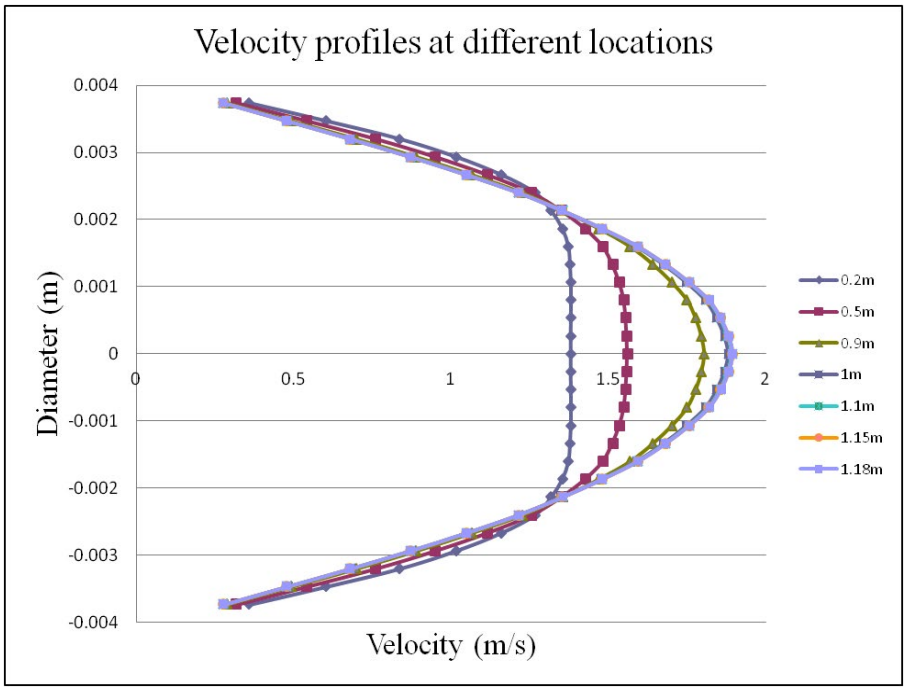


**Figure 11:** Axial velocity profiles at different locations.

Results show variation in axial velocity profiles in the entrance region and as it approaches the parabolic fully-developed profile at around x = 1.1 m.

In the next step, unsteady simulation is performed using a length sufficiently greater than the required entrance length and using pulsating inlet velocity condition. The inlet boundary condition was assigned using a tabular inlet velocity obtained by digitized femoral artery waveform and the liquid properties same as the blood. Since there is time delay in reaching a final velocity profile corresponding to the inlet signal, the simulation is continued for three pulses to obtain more precise results that can be used to compare with the analytical solution.

The results in Figure 12 show comparison with analytical results. As we can see computation results show invariable profiles by the second and the third pulses, approaching a periodic steady condition. In this study, the analysis is concentrated on six different time steps along the different phases of the cardiac cycle: Acceleration phase (0.04sec), Peak systole (0.11sec), deceleration phase (0.2sec), minimum velocity point (0.27sec), diastolic peak (0.5sec) and diastolic phase (0.76sec). Results

show a close agreement between the computational solution and analytical solution. Of particular interest is the profile at t = 0.27s and t = 0.76s that shows two negative reverse flow peaks near the wall and the positive peak at the centerline. These two times locations correspond to the diastolic reverse peak velocity ($V_R$) and the end diastolic velocity ($V_D$) of the inlet velocity waveform.

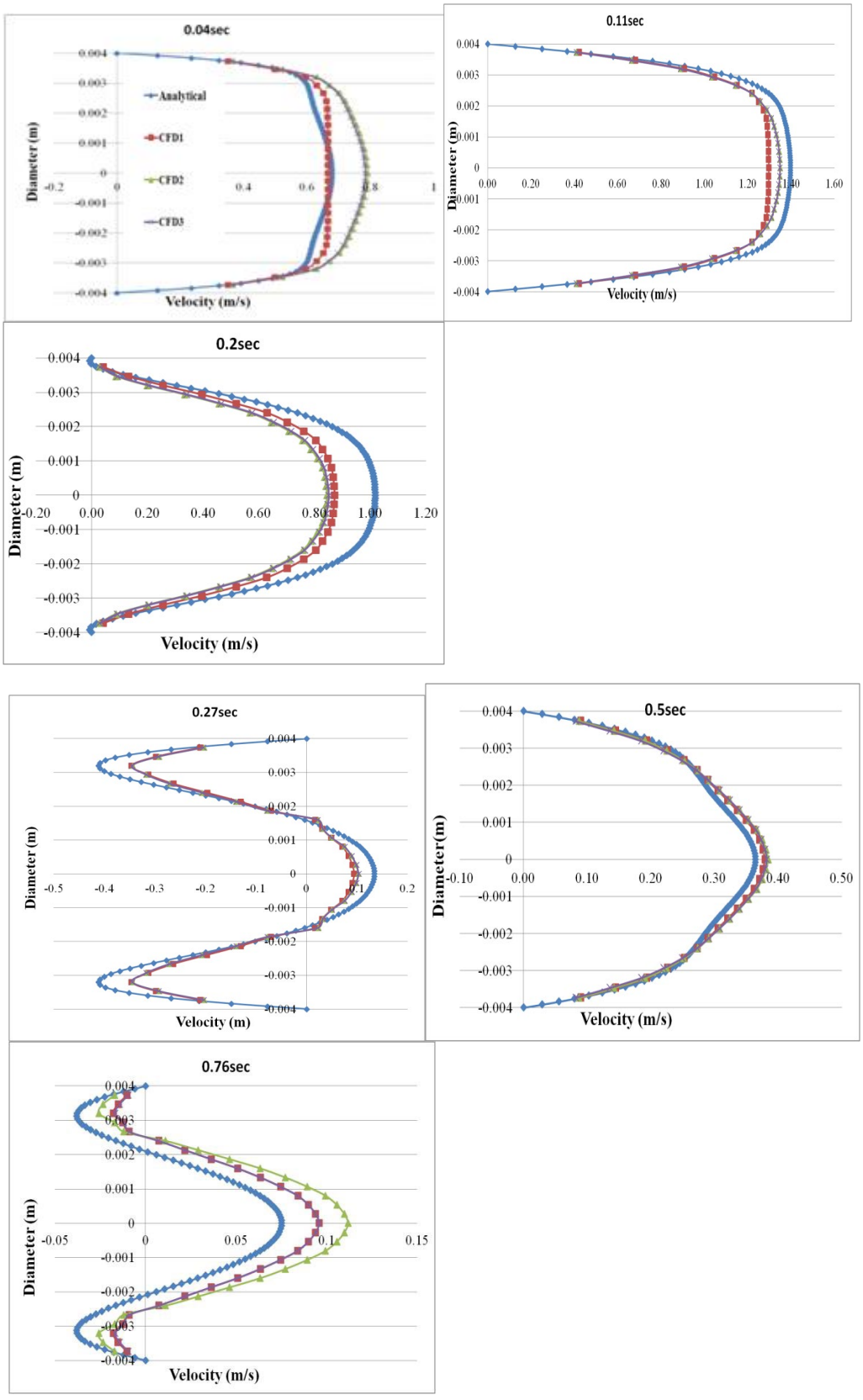


**Figure 12:** Comparison of analytical solutions to CFD along the cardiac cycle.

The axial velocity plots at 1.1m length in a straight section at different time steps in the cardiac cycle are as shown in the Figure 13.

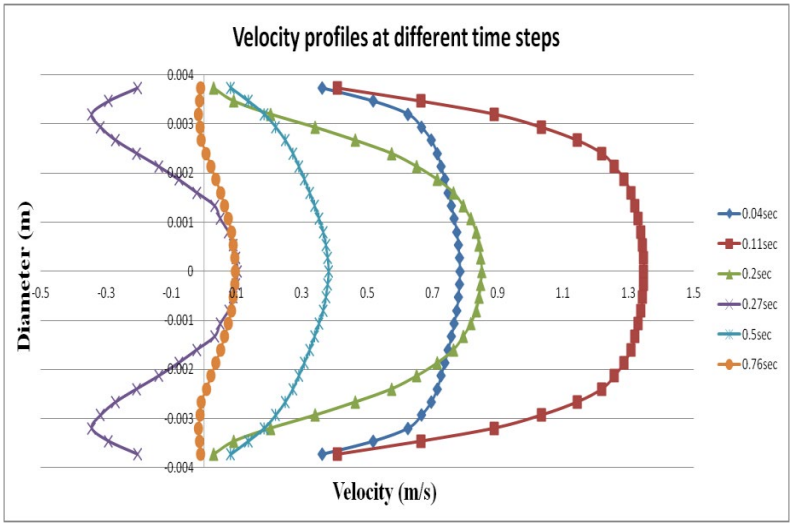


**Figure 13:** Axial velocity profiles at different time steps.

Results in Fig. 13 show that there is a continuous variation in the axial velocity profiles at any location over the periodic cycle in terms of magnitude and shape. Of particular interest is the profiles at t = 0.11s and t = 0.5s that correspond to the two systolic forward peak positive velocity points ($V_F$), and at t = 0.27s and t = 0.76s that corresponds to the two negative diastolic reverse peak velocity points ($V_R$, $V_D$) of the inlet velocity waveform. While profile at t = 0.27s exhibits two distinct parabolic sub-profiles with reverse velocity peaks near the wall, the profile at t = 0.76 show the beginning of the similar two-negative peaks that corresponds to the end of the diastolic velocity ($V_D$).

### 4.2. CFD results of healthy arteries.

Initial simulation results show presence of slow moving re-circulatory regions near the intersection of a main artery and a smaller branch artery and plays major role in the formation of the plaque in arteries. This agrees with the study performed by Silva [4]. Unsteady simulations were performed on an artery section that includes a branch artery section as shown in Figure 5.

The velocity contours at different time steps are shown in Figure 14.

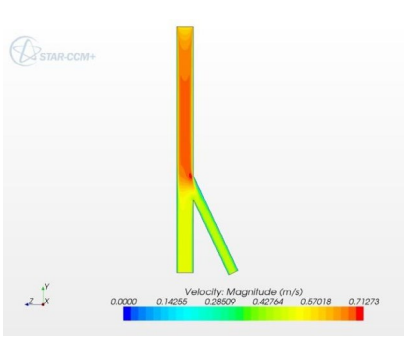


(a) Axial flow velocity contours at 0.04s

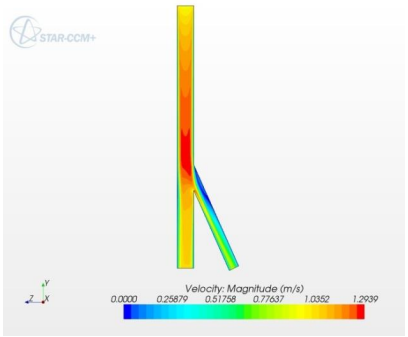


(b) Axial flow velocity contours at 0.11sec

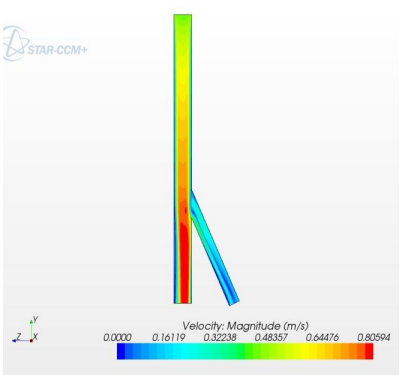


(c) Axial flow velocity contours at 0.2sec

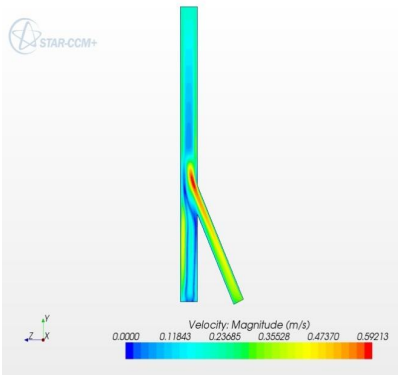


(d) Axial flow velocity contours at 0.27sec

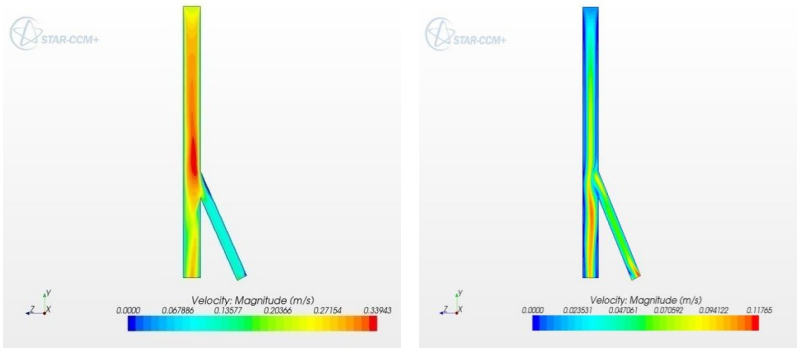


(e) Axial flow velocity contours at 0.5sec (f) Axial flow velocity contours at 0.76sec

**Figure 14:** Axial flow velocity contours at the time steps (a) 0.04sec, (b) 0.11sec (c) 0.2sec (d) 0.27sec E) 0.5sec (f) 0.76sec.

Results show a highly varying flow pattern along the cardiac cycle. The flow at the entrance of the branch shows the occurrence of flow separation and recirculation zones in femoral artery. We can observe the maximum velocity at the wall before the branch is high during the systole period and reduces gradually during the diastolic period of flow, forming the flow separation region at the branch entrance. Since the diastolic flow time is more than the systolic flow, we can say that blood flow patterns during this period are a major contributing factor to the formation of the atherosclerotic plaque at that location. Flow separation and recirculation is stronger at time t = 0.27 (Figure 14d) and t = 0.76 (Figure 14f) that correspond to the two peak negative velocity points of the inlet velocity form.

The Wall Shear Stress (WSS) acting on the arterial walls is plotted against the length of the artery. Shear stress plots at each time steps selected are shown in Figure 15.

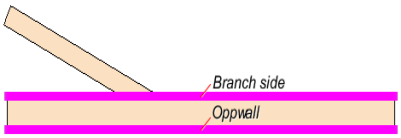


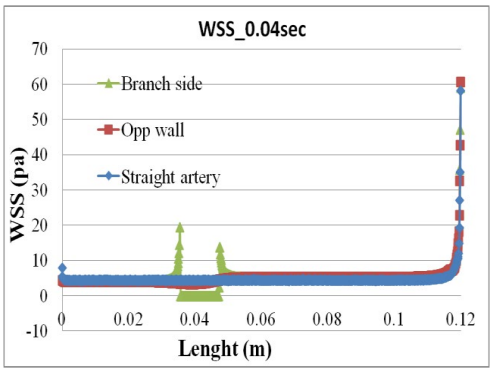


(a) WSS along length of artery 0.04sec

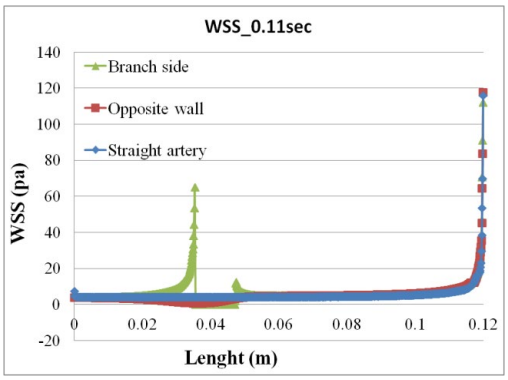


(b) WSS along length of artery 0.11sec

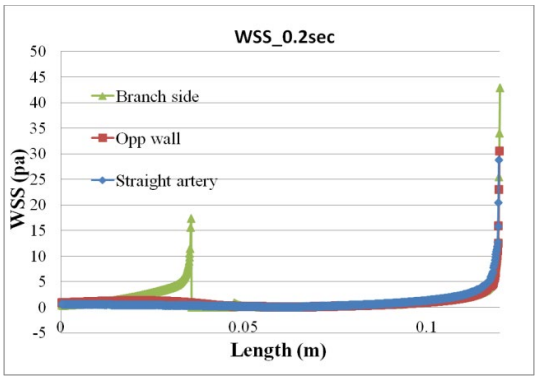


(c) WSS along length of artery 0.2sec

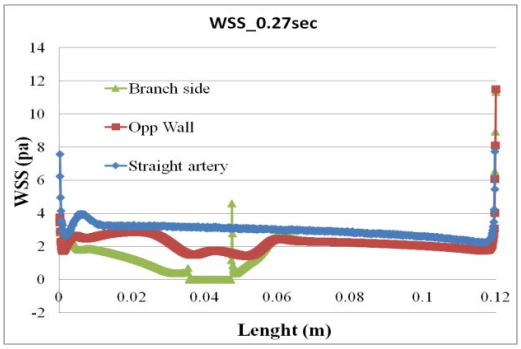


(d) WSS along length of artery 0.27sec

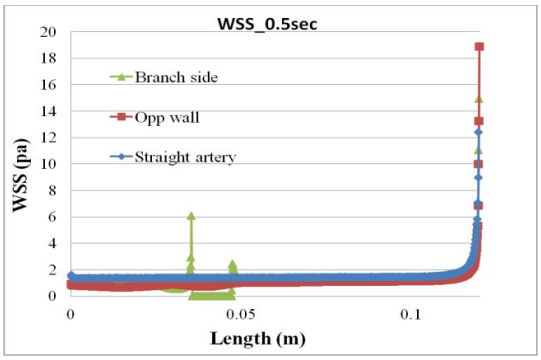


(e) WSS along length of artery 0.5sec

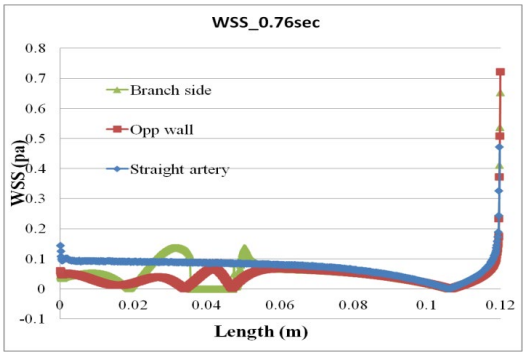


(f) WSS along length of artery 0.76sec

**Figure 15:** Variation of wall shear stress along the length of the artery:
(a) WSS at 0.04s, (b) WSS at 0.11s, (c) WSS at 0.2s, (d) WSS at 0.27s, (e) WSS at 0.5sec and (f) WSS at 0.76sec

Results in Figure 15 show that while Wall Shear Stress (WSS) at the bottom wall symmetrically decrease from the high entrance value to a constant fully developed value, the variation in top wall near the presence of the branch exhibits a significant lower wall shear stress at near 0.27s and 0.76s of the cycle. Observation of results for all time steps reveals that the presence of such low shear stress near the entry of the branch takes place in the diastolic phase (>0.2sec). Such areas with low WSS are the feasible locations for formation of plaques. Since the time of diastolic phase is more than that of the systolic phase, the wall before the arterial branch will be experiencing the low shear stresses for longer duration of time. Based on this, we can

conclude that the area before the branch is feasible for initiation of the stenosis (Atherosclerotic plaque) due to the presence of slow-moving regions and presence of lower wall shear stress. We can also conclude that arterial geometry plays a major role in the initiation of the atherosclerotic plaque.

### 4.3. CFD analysis of stenosis effected artery.

While this study does not include any two-phase analysis with deposition and dynamic formation of plaque on artery surface, blood flow analysis is performed to characterize the flow conditions and stresses on arteries with the formation of plaque, a condition known as stenosis affected artery.

A stenosis affected artery region may form near the entrance to a branch over period. To characterize the flow in a stenosis affected region, a region with 50% restriction in flow region is considered to replicate artery section with plaque formation. CFD simulation results of the stenosis effected artery reveal the flow disturbances caused due to the restriction of the flow. Figure 16 illustrates the flow distribution of the stenosis affected artery along the cardiac cycle.

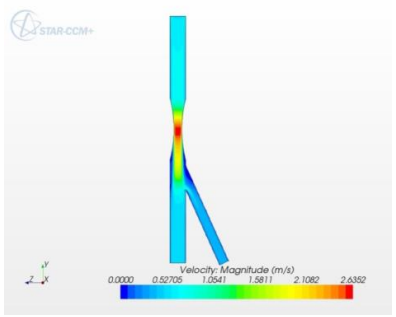


(a) Velocity distribution at 0.04 sec

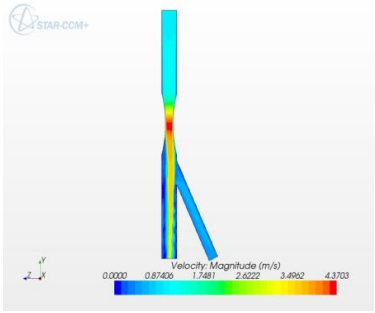


(b) Velocity distribution at 0.11 sec

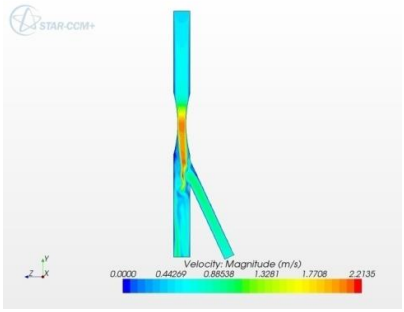


(c) Velocity distribution at 0.2 sec

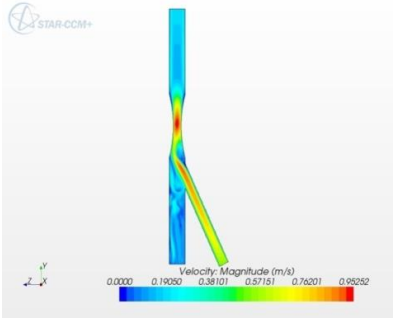


(d) Velocity distribution at 0.27 sec

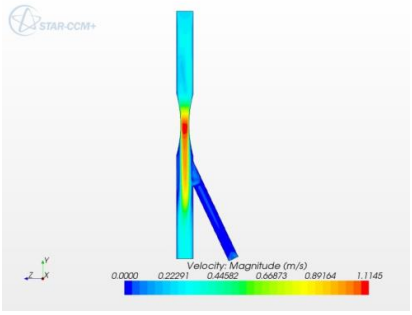


(e) Velocity distribution at 0.5 sec

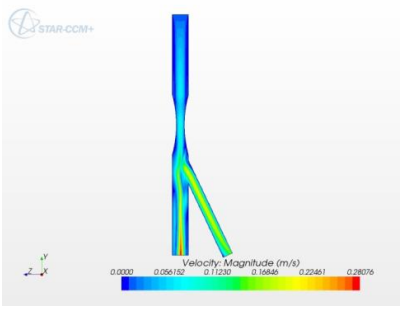


(f) Velocity distribution at 0.76 sec

**Figure 16:** Velocity contour of restricted artery along the cardiac cycle.

From Figure16 we can observe the flow disturbances caused due to the restriction of the artery. A much stronger recirculation zones are formed at the entrance of the branch as compared to the healthy artery. This indicates that it may a take long time to initiate the plaque formation, but once the restriction is formed it takes less time to increase the percentage of restriction as well as growth in the leading and trailing end due to the presence of the slow moving recirculatory regions.

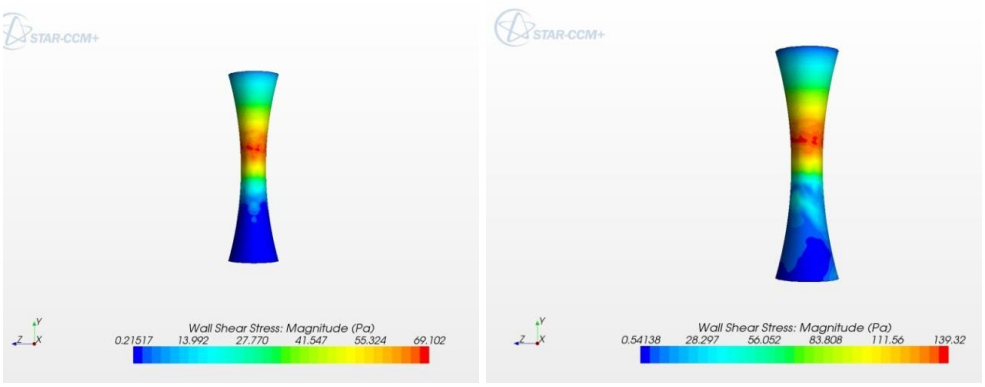


(a) WSS at the restriction at 0.04sec (b) WSS at the restriction at 0.11sec

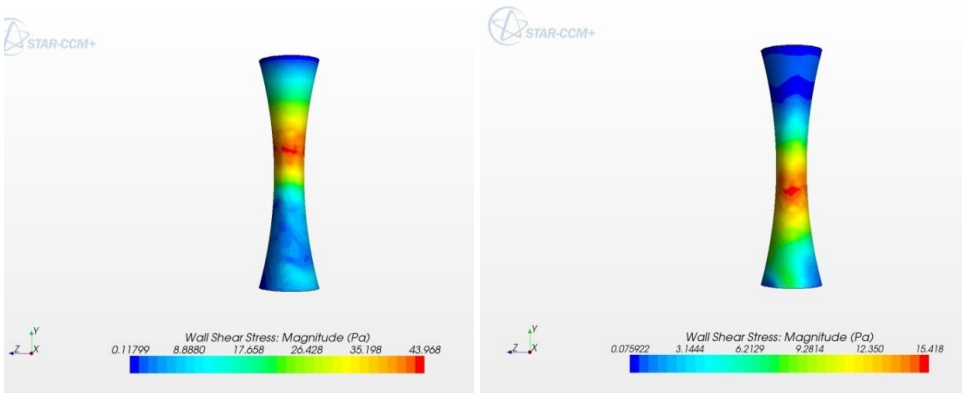


(c) WSS at the restriction at 0.2sec (d) WSS at the restriction at 0.27sec

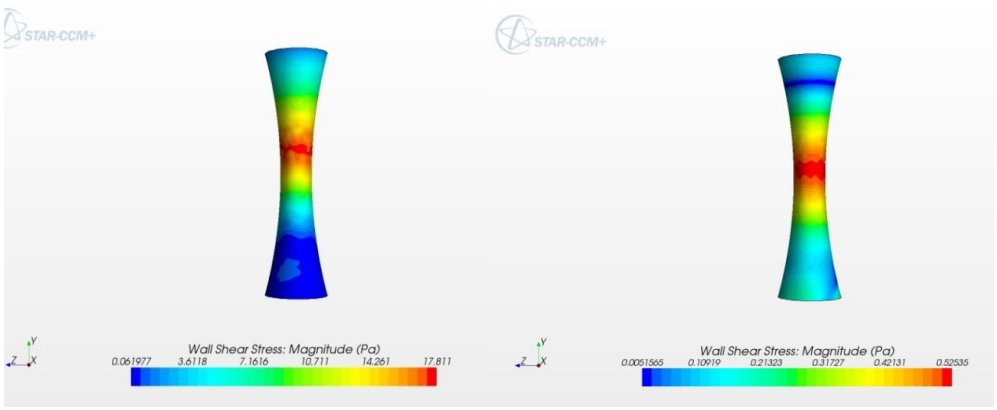


(e) WSS at the restriction at 0.5sec (f) WSS at the restriction at 0.76sec

**Figure 17:** WSS distribution at the restriction of the artery.

Figure 17 shows the WSS distribution in the restricted zone along the cardiac cycle. By observation we can conclude that the WSS distribution is high at the middle of the section along the cardiac cycle but varies at the corners of the restricted zone where the formation of the plaque is likely to be more. This adds support to the conclusion in the above section that it may take a long time to initiate the plaque formation but once the plaque is formed it may grow and increase the blockage of the artery at a faster rate.

The mean velocity across the peak restriction of the artery is plotted against the time along the cardiac cycle. Figure 18 shows the comparison between the mean velocities across the artery at the peak restriction for the stenosis effected and mean velocity distribution across the artery at the same location for the healthy artery.

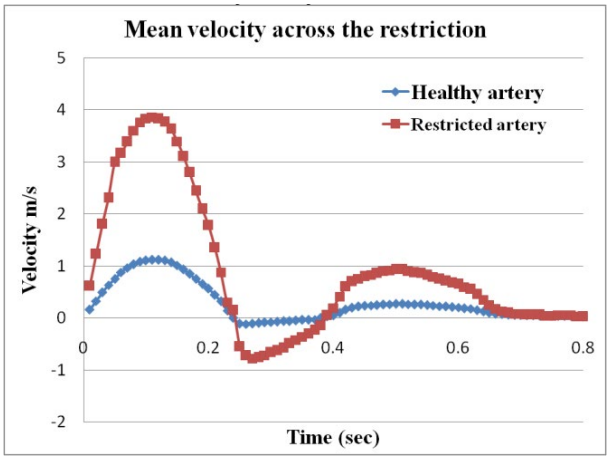


**Figure 18:** Mean velocity across the restriction for both healthy and restricted artery along the cardiac cycle.

The velocity distribution in the restricted zone exhibits a higher velocity fluctuation with significantly higher peak positive and negative velocities as compared to the velocity distribution for the healthy artery.

### 4.4. CFD analysis stented artery

Simulations were conducted on the stented artery to Figure out the differences in the flow characteristics among healthy, stenotic and stent implanted arteries. In this study, flow distribution in two types of stents with strut space 3mm and 1.5 mm are considered.

#### 4.4.1. Stented artery with 3mm strut spacing.

The velocity distribution along the cardiac cycle in the stented artery with stent of strut spacing 3mm is shown in Figure 19 and an enlarged view in Figure 20.

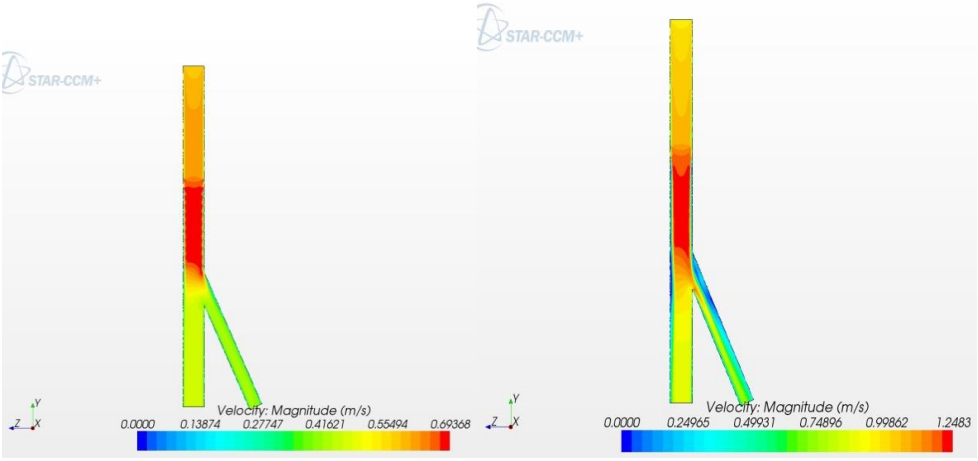


(a) Velocity contour at 0.04 sec

b)) Velocity contour at 0.11sec

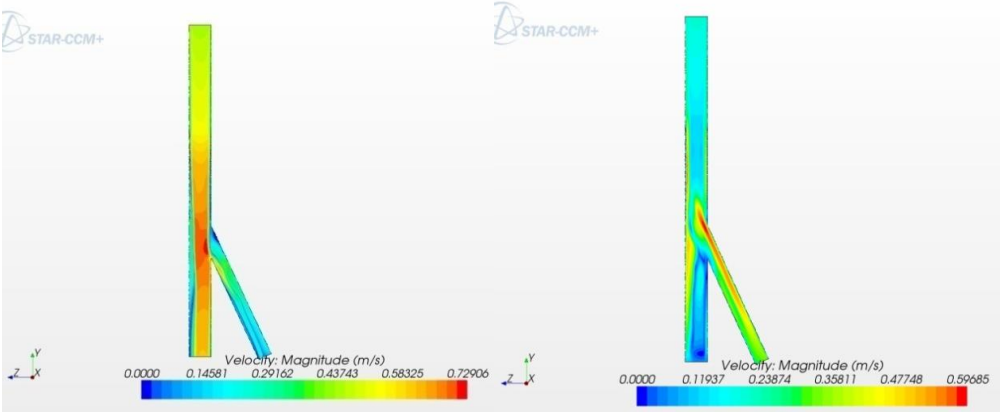


(c)Velocity contour at 0.2sec

(d) Velocity contour at 0.27sec

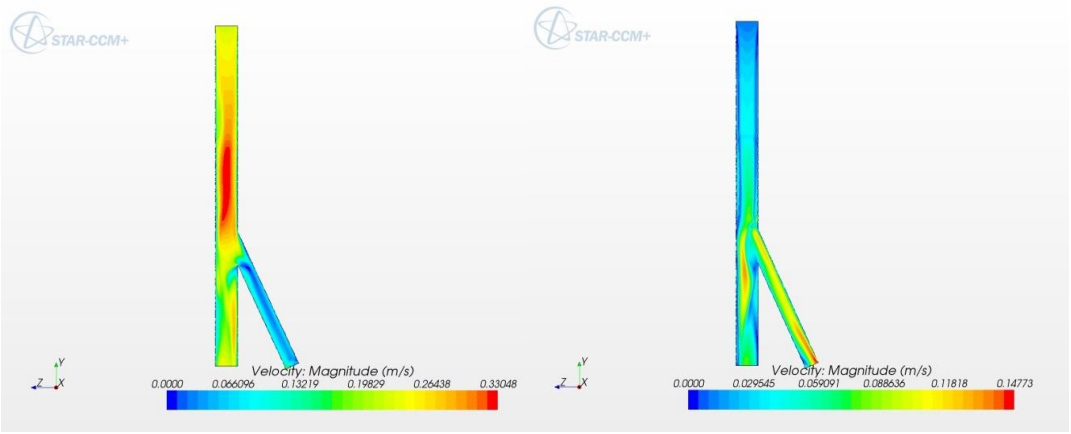


(e) Velocity contour at 0.5sec (f) Velocity contour at 0.76sec

**Figure 19:** Velocity contours of stented artery of 3mm strut space.

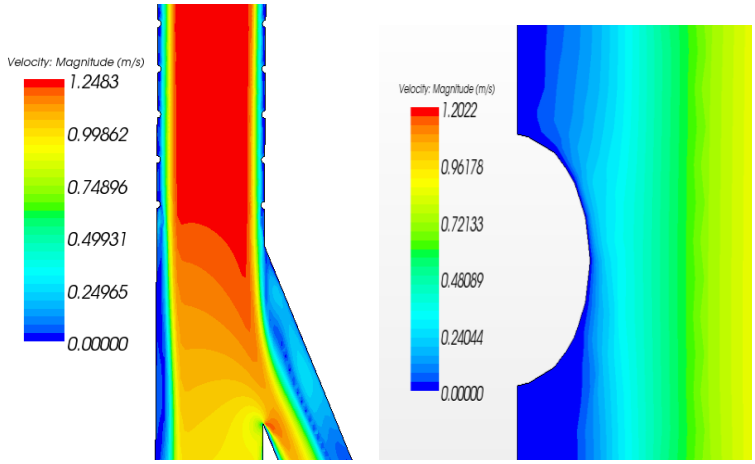


**Figure 20:** Enlarged view of the stented artery with 3mm strut space.

From Figures 14 and 19 we can compare the contour velocity plots between healthy artery and stented artery. Results show that, in the presence of stent it exhibits a similar flow region in the core region and almost regulated as expected in healthy artery. However, flow regions near the stent wall and the cavity regions in between strut involves slow moving fluid and periodic variation in the axial velocity profile near the wall. Slow moving regions near the stent wall can be seen in Figure 20.

WSS distribution on the stent surface along the cardiac cycle is as shown in Figure 21.

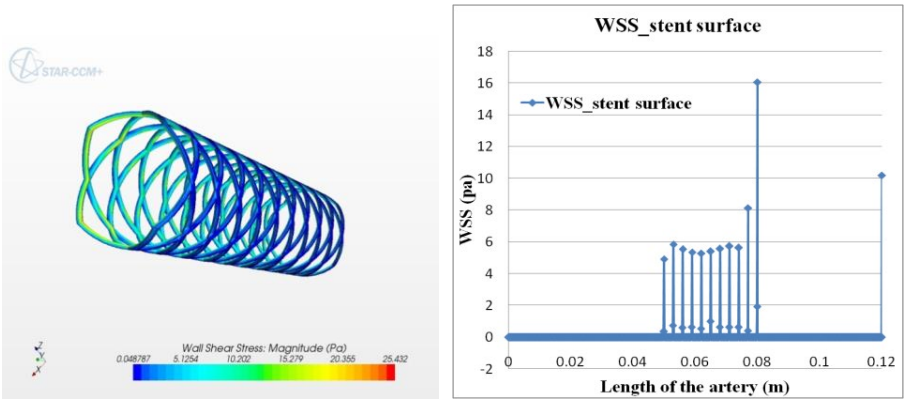


(a) WSS at 0.04sec

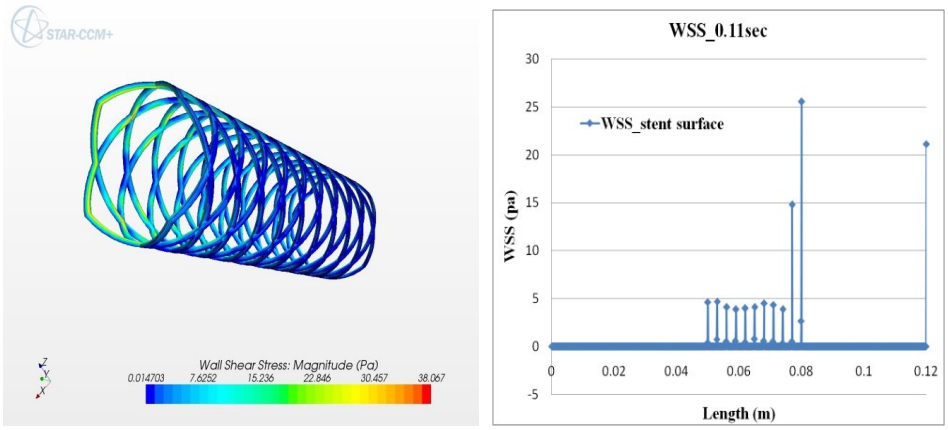


(b) WSS contour and distribution along the of stent at 0.11sec

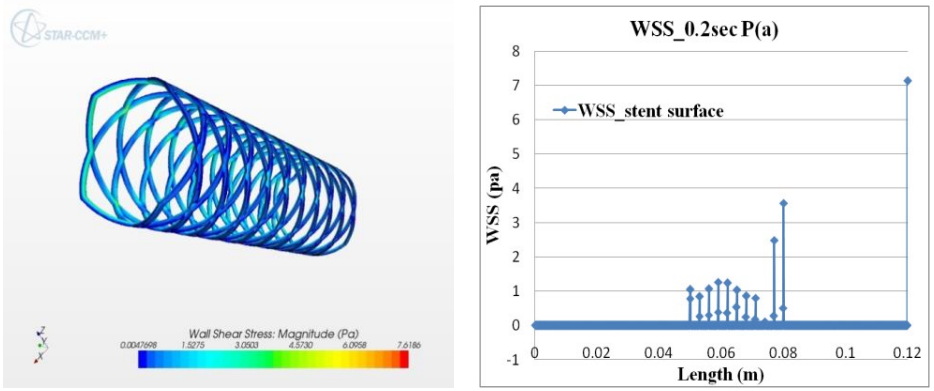


(c) WSS contour and distribution along the stent at 0.2sec

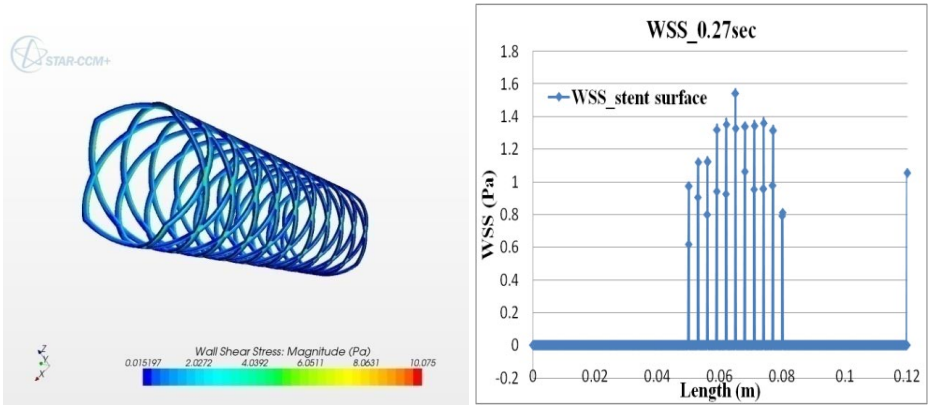


(d) WSS contour and distribution along the stent at 0.27sec

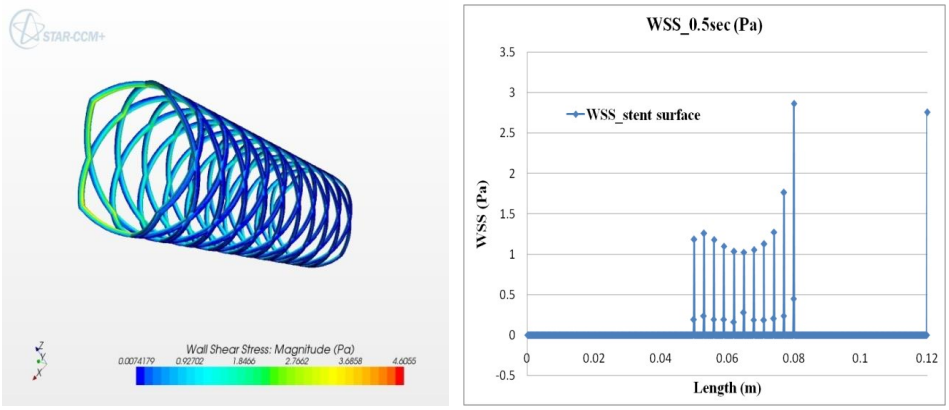


(e) WSS contour and distribution along the stent at 0.5sec

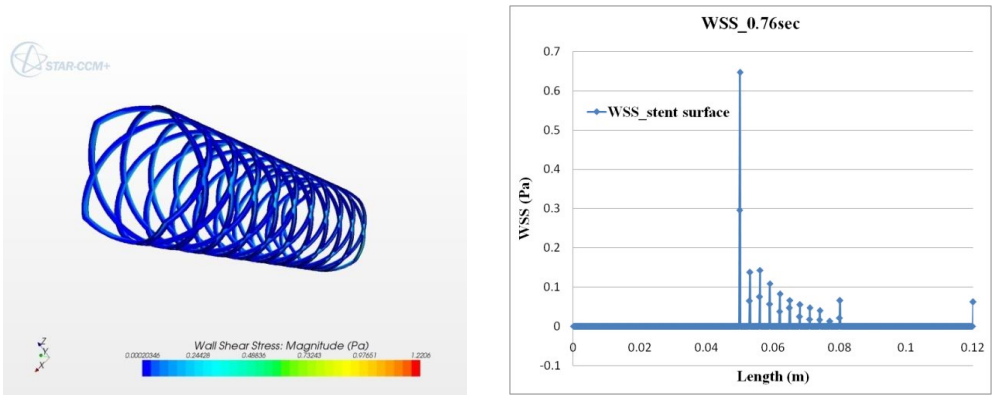


(f) WSS contour and distribution along the stent at 0.76sec

**Figure 21:** WSS distribution on the stent surface for stent with 3mm strut space along the cardiac cycle.

From Figure 21 we can observe the WSS along the walls of the stent are decreasing in the flow direction during systole and increasing in the flow direction during the diastole. The WSS acting on the walls of the stent is not the same for the boys. This complex behavior of the WSS might be helpful in designing the drug eluting stent to decide the quantity of the coating.

### 4.5. Comparison of WSS on stent with 3mm and 1.5 mm strut space

WSS acting on the artery wall along the cardiac cycle with stent implanted on it is as shown in Figure 22. In Figure 4.16 green represents the WSS for the 3mm stent and red represents the 1.5mm stent.

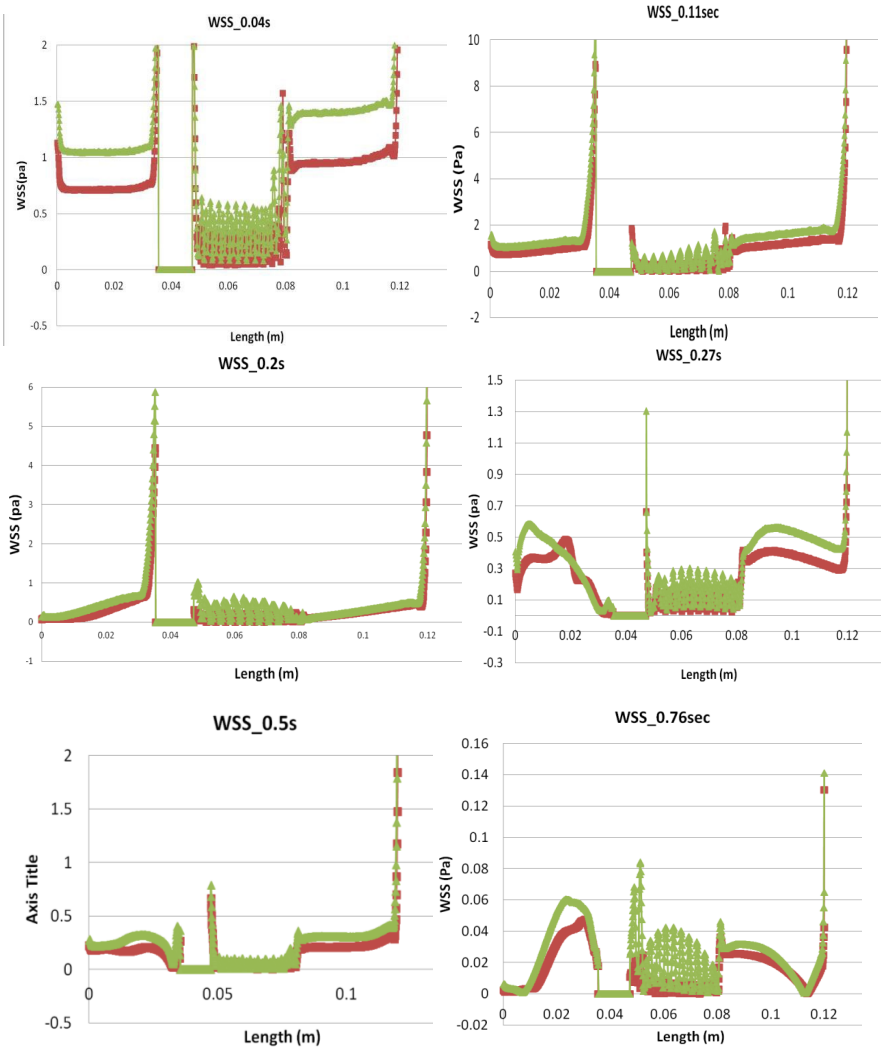


**Figure 22:** WSS distribution along the length of the wall in both 1.5mm and 3mm strut spacing.

From the above figure, we can conclude that the WSS on the walls of the artery with stent 3mm strut space is more than the artery with stent 1.5mm strut space. This results in more possibility of formation of restenosis in stent with strut space 1.5. Strut spacing should be one of the criteria in designing the stent. The contour plot for the WSS acting on the wall of the artery at the stent location is shown in Figure 23.

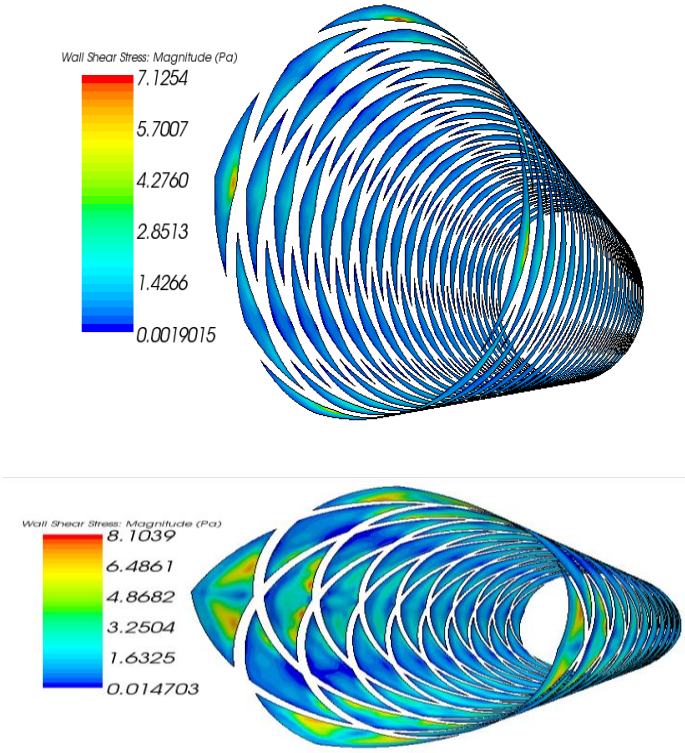


**Figure 23:** WSS acting on the arterial wall at the stent location at peak systole in the cardiac cycle.

From Figures 22 and 23, we can conclude that the WSS acting on the walls of the arteries is more in stent with strut space 3mm.

## 5. Conclusion

A blood flow dynamic model is developed to simulate hydrodynamic and stress field conditions in a human femoral artery over a cardiac cycle developed by the heartbeats. Simulations are performed on three different conditions: *healthy, atherosclerosis affected* and *stented* femoral arteries to analyze the velocity and wall shear stress fields developed within the artery. Such a simulation model is essential to predict the outcome of the interventions in terms of recirculation and stagnation regions and identify improved stent designs. It has been demonstrated that (a) The flow patterns in the arteries are highly modulating along the cardiac cycle and a strong function of the waveform created by the heartbeat; (b) The complex blood flow pattern with slow moving regions, flow separation and recirculatory regions during cardiac cycle is the major contributing factor to the formation of the atherosclerotic plaque; (c) The arterial geometry plays a major role in the initiation of the atherosclerotic plaque; (d) The flow regions near the stent wall and the cavity regions in between strut involve slow moving fluid along with a periodic variation in the axial velocity profile near the wall; (e) The complex behavior of the induced wall shear stress (WSS) is a critical factor for designing and developing stents as well as the drug eluting stents in terms of strut size and spacing in prevention restenosis.

## References


1. Womersley, J. R. (1955). Method for the calculation of velocity, rate of flow and viscous drag in arteries when the pressure gradient is known. *The Journal of physiology, 127*(3), 553.
2. McDonald, D. A. (1955). The relation of pulsatile pressure to flow in arteries. *The Journal of physiology, 127*(3), 533.
3. Hale, J. F., McDonald, D. A., & Womersley, J. R. (1955). Velocity profiles of oscillating arterial flow, with some calculations of viscous drag and the Reynolds number. *The Journal of physiology, 128*(3), 629.
4. Ku, D. N. (1997). Blood flow in arteries. *Annual review of fluid mechanics, 29*(1), 399-434.
5. Silva, E., Teixeira, S., & Lobarinhas, P. (2010). Computational fluid dynamics simulations: An approach to evaluate cardiovascular dysfunction. *University of Minho., Portugal, Europe,* 25-46.
6. Taylor, C. A., & Draney, M. T. (2004). Experimental and computational methods in cardiovascular fluid mechanics. *Annu. Rev. Fluid Mech., 36*, 197-231.
7. Pant, S., Bressloff, N. W., Forrester, A. I., & Curzen, N. (2010). The influence of strut-connectors in stented vessels: a comparison of pulsatile flow through five coronary stents. *Annals of biomedical engineering, 38,* 1893-1907.
8. Jin, S., Yang, Y., Oshinski, J., Tannenbaum, A., Gruden, J., & Giddens, D. (2004, September). Flow patterns and wall shear stress distributions at atherosclerotic-prone sites in a human left coronary artery-an exploration using combined

methods of CT and computational fluid dynamics. In *The 26th Annual International Conference of the IEEE Engineering in Medicine and Biology Society* (Vol. 2, pp. 3789-3791). IEEE.
9. Dehlaghi, V., Najarian, S., & Tafazzoli-Shadpor, M. (2008, February). Effect of the length, curvature and stent geometry on restenosis in stented human coronary artery. In *ACTA CARDIOLOGICA* (Vol. 63, No. 1, pp. 119-119).
10. He, X., Ku, D. N., & Moore, J. E. (1993). Simple calculation of the velocity profiles for pulsatile flow in a blood vessel using Mathematica. *Annals of biomedical engineering, 21*, 45-49.
11. Hashimoto, J., & Ito, S. (2010). Pulse pressure amplification, arterial stiffness, and peripheral wave reflection determine pulsatile flow waveform of the femoral artery. *Hypertension, 56*(5), 926-933.
12. Wong, H. C., Cho, K. N., & Tang, W. C. (2009, October). Bending of a stented atherosclerotic artery. In *Comsol Conference, Boston.*
13. Shaik, E., Hoffmann, K., & Dietiker, J. F. (2006). Numerical flow simulations of blood in arteries. In *44th AIAA Aerospace Sciences Meeting and Exhibit* (p. 294).
14. Dehlaghi, V., Tafazzoli-Shadpour, M., & Najarian, S. (2007). Numerical analysis of pulsatile blood flow in a stented human coronary artery with a flow divider. *American Journal of Applied Sciences, 4*(6), 397-404.
15. Yang, H., & Kim, K. S. (2011, January). Numerical Hemodynamics Analysis of Stented Cerebral Artery. In *ASME International Mechanical Engineering Congress and Exposition* (Vol. 54884, pp. 271-277).
16. Valencia, A., & Villanueva, M. (2006). Unsteady flow and mass transfer in models of stenotic arteries considering fluid-structure interaction. *International Communications in Heat and Mass Transfer, 33*(8), 966-975.
17. Cole, J. S., Gillan, M. A., Raghunathan, S., & O'reilly, M. J. G. (1999). Numerical Simulations of Time-Dependent, non-Newtonian Blood Flow through Typical Human Arterial Bypass Grafts. *Developments in Chemical Engineering and Mineral Processing, 7*(1-2), 179-200.
18. National Heart Lung and Blood Institute, "Anatomy of the heart" http://www.nhlbi.nih.gov/health/health-topics/topics/hhw/anatomy.html
19. A detail network of arteries and vein a human blood circulatory system [encyclopedia: https://cdn.britannica.com/49/115249-050-0DFBBCD3/Human-circulatory-system.jpg]
20. Watson, T., Webster, M. W., Ormiston, J. A., Ruygrok, P. N., & Stewart, J. T. (2017). Long and short of optimal stent design. *Open Heart, 4*(2), e000680.
21. Schmitz, K. P., Behrend, D., Behrens, P., & Schmidt, W. (1999). Comparative studies of different stent designs. *Prog Biomed Res, 4,* 52-58.
22. Wawrzyńska, M., Arkowski, J., Włodarczak, A., Kopaczyńska, M., & Biały, D. (2018). Development of drug-eluting stents (DES). In Functionalised Cardiovascular Stents (pp. 45-56). Woodhead Publishing.
23. Stoeckel, D., Bonsignore, C., & Duda, S. (2002). A survey of stent designs. *Minimally Invasive Therapy & Allied Technologies, 11*(4), 137-147.
24. Noad, R. L., Hanratty, C. G., & Walsh, S. J. (2014). Clinical impact of stent design. *Interventional Cardiology Review, 9*(2), 89.
25. Schmidt, T., & Abbott, J. D. (2018). Coronary stents: history, design, and construction. *Journal of clinical medicine, 7*(6), 126.
26. Van de Vosse, F. N., & Stergiopulos, N. (2011). Pulse wave propagation in the arterial tree. *Annual Review of Fluid Mechanics, 43,* 467-499.
27. National Heart Lung and Blood Institute, "Anatomy of the heart" http://www.nhlbi.nih.gov/health/health-topics/topics/hhw/anatomy.html
28. Articles of Heart, "Heart Rate Chart" http://www.heart.com/heart-rate-chart.html
29. Encyclopedia Britannica, "Human Circulatory System" http://www.britannica.com/bps/media-[view/141810/1/0/0]
30. Blood Vessels. "Structure of blood vessels Walls," http://www.rci.rutgers.edu/~uzwiak/AnatPhys/Blood_Vessels.html
31. Ghasemalizadeh, O., Mirzaee, M., & Firoozabadi, B. (2012). Modeling the human cardiovascular system and peristaltic motion of descending arteries using the lumped method. Internet J Bioeng, 3, 1-11.
32. National Heart Lung and Blood Institute, "Coronary Heart Disease"http://www.nhlbi.nih.gov/health/health-topics/topics/cad/
33. National Heart Lung and Blood Institute, "Angioplasty" http://www.nhlbi.nih.gov/health/health-topics/topics/angioplasty/